

# Accelerating Generalized Linear Models with MLWeaving: A One-Size-Fits-All System for Any-precision Learning

Zeke Wang, Kaan Kara, Hantian Zhang, Gustavo Alonso, Onur Mutlu, Ce Zhang  
Systems Group, Department of Computer Science  
ETH Zurich, Switzerland  
firstname.lastname@inf.ethz.ch

## ABSTRACT

Learning from the data stored in a database is an important function increasingly available in relational engines. Methods using lower precision input data are of special interest given their overall higher efficiency but, in databases, these methods have a hidden cost: the quantization of the real value into a smaller number is an expensive step. To address the issue, in this paper we present MLWeaving, a data structure and hardware acceleration technique intended to speed up learning of generalized linear models in databases. MLWeaving provides a compact, in-memory representation enabling the retrieval of data at any level of precision. MLWeaving also takes advantage of the increasing availability of FPGA-based accelerators to provide a highly efficient implementation of stochastic gradient descent. The solution adopted in MLWeaving is more efficient than existing designs in terms of space (since it can process any resolution on the same design) and resources (via the use of bit-serial multipliers). MLWeaving also enables the runtime tuning of precision, instead of a fixed precision level during the training. We illustrate this using a simple, dynamic precision schedule. Experimental results show MLWeaving achieves up to  $16\times$  performance improvement over low-precision CPU implementations of first-order methods.

### PVLDB Reference Format:

Zeke Wang, Kaan Kara, Hantian Zhang, Gustavo Alonso, Onur Mutlu, Ce Zhang. Accelerating Generalized Linear Models with MLWeaving: A One-Size-Fits-All System for Any-precision Learning. *PVLDB*, 12(xxx): xxxx-yyyy, 2019.  
DOI: <https://doi.org/TBD>

## 1. INTRODUCTION

It is widely adopted by databases to support for training machine learning (ML) models over relational data (e.g., MADlib [33]). We focus on one of the most popular ML models in databases: Generalized linear models, such as support vector machines and logistic regression, solved using stochastic gradient descent (SGD). A further ongoing trend in ML nowadays is quantization: For instance, it is applied to weights in deep neural networks to reduce model sizes [17, 32, 82] or, as we focus in this work, input datasets are quantized directly to reduce the amount of data accessed during

Permission to make digital or hard copies of all or part of this work for personal or classroom use is granted without fee provided that copies are not made or distributed for profit or commercial advantage and that copies bear this notice and the full citation on the first page. To copy otherwise, to republish, to post on servers or to redistribute to lists, requires prior specific permission and/or a fee. Articles from this volume were invited to present their results at The 45th International Conference on Very Large Data Bases, August 2019, Los Angeles, California.

*Proceedings of the VLDB Endowment*, Vol. 12, No. xxx  
Copyright 2018 VLDB Endowment 2150-8097/18/10... \$ 10.00.  
DOI: <https://doi.org/TBD>

training, shortening training times [96]. Existing approaches using the latter technique either assume that the data is always available in the correct precision (e.g., for 32-bit fixed-point numbers, 32 versions of the original data with precision ranging from 1 to 32 bits are required), or assume that the data is quantized at its source (e.g., memory or disk) [19, 44]. A further challenge is that the correct precision is not always known in advance and varies depending on statistical characteristics of the dataset. The overhead for quantized learning is even bigger when hardware accelerators are used, since existing solutions require a different microarchitecture for each precision [44] in addition to a separate copy of quantized data being available at the right level of precision.

To address these issues and unleash the full potential of quantized learning, we have designed MLWeaving, a novel *end-to-end* system (C1) enabling *any-precision* learning of generalized linear models. MLWeaving is based on two key innovations to make the learning process quantization-friendly: A novel flexible memory layout and a specialized FPGA-based architecture. Combining these two components enables the capability to dynamically adjust the precision used during training. We illustrate the benefit of such capability using a simple dynamic, per-epoch precision schedule (we leave the exploration of more efficient dynamic schedules to future work). A further contribution is an efficient synchronous computation scheme built into the hardware accelerator (C2), making training more appealing on FPGAs when compared with other devices such as CPUs or existing designs requiring different circuits for each level of precision. Finally, we have an initial integration of MLWeaving in a column store database (DoppioDB) as a first step to explore how database storage formats can be combined with the requirements of machine learning algorithms.

### C1: Flexible Memory Layout and Hardware Implementation.

The key idea of MLWeaving is a transposed memory layout where different bits of a given value are stored separately. MLWeaving vertically partitions each data point (a row in a table) at the bit level. Such an approach is based on the observation that SGD is evaluated *sample-at-a-time*, i.e., all the features of the sample are read before the gradient is computed. This provides two benefits. First, the number of memory accesses needed to read a value is proportional to the precision used. Lower precision leads to fewer memory accesses. Second, the format allows the serialization of the data into a hardware accelerator in the form of a bit stream, which improves the memory bandwidth utilization - a typical problem on hardware accelerators connected through a PCI interface such as the one we use in this paper, an FPGA. We show that the bit stream format can be used to compute the gradient using bit-serial multipliers (i.e., process all the first bits in the first cycle, all the second bits in the second cycle, etc. [42, 63, 78, 83, 92, 93]) a more efficient approach than that used in existing systems [19, 44]. The resulting

design employs only one third of the resources used in previous solutions and allows higher frequency, doubling the rate at which data can be processed on an FPGA accelerator. Furthermore, our approach supports dynamic selection of the level of precision by simply reading more or fewer bits when processing the data in each epoch of the SGD algorithm. We illustrate the benefit of this by using a simple per-epoch dynamic precision scheduling.

**C2: Efficient Synchronous Execution.** Due to the sequential nature of the SGD algorithm, a common approach to parallelize it on modern CPUs/GPUs is to perform asynchronous updates to the model. By doing so, different threads do not need to acquire expensive locks for every gradient calculation [70, 97]. Such approaches are guaranteed to converge under certain constraints, but the stale model used to compute the gradients causes the algorithm to require more epochs to converge. MLWeaving allows designers to use synchronous SGD on the FPGA with performance similar to its asynchronous SGD on the FPGA. Since synchronous SGD is more robust and has better statistical properties along a wider range of use cases than its asynchronous counterparts, MLWeaving removes the performance motivation for less robust approaches. As a result, MLWeaving requires significantly fewer epochs to converge while each epoch requires a similar amount of time as its asynchronous CPU counterpart. For example, MLWeaving with a 3-bit precision requires only 40 epochs to converge for the dataset Epsilon, while the full-precision CPU counterpart needs at least 199 epochs to converge to the same loss in Figure 15a.

We implement MLWeaving on an Intel Arria 10 FPGA using Intel’s Xeon+FPGA platform (HARP) where the FPGA is integrated in the same package as a Xeon multicore CPU. Experimental results show that MLWeaving achieves up to  $16\times$  performance improvement over the state-of-the-art low-precision first-order CPU implementation in Table 8.

## 2. BACKGROUND

MLWeaving combines ideas from several areas: databases, machine learning, and computer architecture. In this section we introduce the necessary background to understand the overall design. Table 1 summarizes the notation used throughout the paper.

### 2.1 Quantization and Low Precision Arithmetic

For all ML algorithms, raw data must be converted into a suitable format before the learning process. In MLWeaving, data is stored in the format resulting from a normalization and a quantization step.

Normalization reduces the range of values without affecting the overall result of the training. Without loss of generality, MLWeaving uses the scaled range:  $[0, 1]$ . Accordingly, for each column, the original value ( $f$ ) is normalized to the value ( $\tilde{f}$ ), as shown in Equation 1:

$$\tilde{f} = \frac{f - f_{min}}{f_{max} - f_{min}}, \quad (1)$$

where  $f_{min}$  and  $f_{max}$  are the maximum and minimum values in the column, respectively. An advantage of learning inside the database engine is that normalization can be accomplished using either the meta-data available on a relational table or computed using standard SQL (min, max).

Quantization happens over the normalized dataset. It involves converting a full-precision floating-point value (e.g.,  $\tilde{f}$ ) into a lower-precision fixed-point value. Specifically, our goal is to construct a function  $Q_s : \mathbb{R}^d \mapsto \mathbb{F}^d$ , a *deterministic quantization function* that maps a floating-point value to an  $s$ -bit fixed-point representation  $Q_s(a)$ . The quantization process can be conducted in two steps.

**Floating Point to Fixed Point Conversion.** The first step is to generate a *full-precision fixed-point table*  $T_S$ , where  $S$  is the

1st row	ABCD	EFGH	IJKL	MNOP	RSTU	VXYZ	1010	0101
2nd row	abcd	efgh	ijkl	mno	rstu	vxyz	1100	0011

(a) Full-precision fixed-point table  $T_S = T_4$

1st row	ABC	EFG	IJK	MN	RST	VXY	101	010
2nd row	abc	efg	ijk	mno	rst	vxy	110	001

(b) 3-bit fixed-point table  $T_3$

1st row	AB	EF	IJ	M	RS	VX	10	01
2nd row	ab	ef	ij	m	rs	vx	11	00

(c) 2-bit fixed-point table  $T_2$

1st row	A	E	I	M	R	V	1	0
2nd row	a	e	i	m	r	v	1	0

(d) 1-bit fixed-point table  $T_1$

Figure 1: Four fixed-point quantized tables ( $T_4, T_3, T_2, T_1$ ). Each table has two rows and eight columns, and each element has four bits, where the symbol (e.g., A-Z, a-z) is binary, 0 or 1.

maximum number of bits of the quantized value in the table. The new fixed-point value ( $\tilde{a}$ ) in  $T_S$  is calculated to be  $\tilde{f}$  multiplied by  $2^S - 1$  (instead of  $2^S$ )<sup>1</sup>, since the range of each floating-point value in the normalized table is between 0 and 1. Therefore, the larger the  $S$  value, the higher the precision. In our FPGA design, the fixed-point value  $\tilde{a}$  is interpreted as:

$$\tilde{a} = \sum_{i=1}^S \tilde{a}^{[i]} \times 2^{-i}, \quad (2)$$

where  $\tilde{a}^{[i]}$  represents the  $i$ -th bit of  $\tilde{a}$ , 0 or 1. The first bit ( $i = 1$ ) is the most significant bit. Figure 1(a) shows an example of a full-precision fixed-point table  $T_S$  where  $S = 4$ . The quantized value ( $\tilde{a} = 1010_2$ ) of the seventh column and the first row<sup>2</sup> represents the value of  $\tilde{f}$ :  $1 \times 2^{-1} + 0 \times 2^{-2} + 1 \times 2^{-3} + 0 \times 2^{-4} = 0.625$ .

**Fixed Point Quantization.** The second step of  $Q_s$  is to quantize the fixed point table  $T_S$  into the desired level of precision. This step is done by taking the  $s$  most significant bits out of  $T_S$ . Figures 1(b-d) illustrates the quantized 3-bit, 2-bit and 1-bit fixed-point tables for the original data shown in Figure 1(a). For example, the full-precision fixed point representation  $1010_2$  in  $T_4$  is  $101_2$ ,  $10_2$ , and  $1_2$  for 3, 2, and 1 bit precision, respectively.

### 2.2 Low-precision Stochastic Gradient Descent

SGD is a popular algorithm to train generalized linear models. Given a relation  $A$ , the full precision SGD solves the optimization problem:

$$\text{minimize} : \frac{1}{N} \sum_{i=1}^N f(\vec{x} \cdot \vec{a}_i, b_i),$$

where  $\vec{a}_i$  is one row in the input relation,  $b_i$  is the corresponding training label,  $\vec{x}$  is the model, and  $f(-)$  is a loss function. SGD solves this problem by iteratively scanning the input relation  $A$  – for each row  $\vec{a}_i$ , it calculates the gradient with respect to  $\vec{x}$ , and updates the model. Each pass over the input data is called an *epoch*. SGD usually runs for multiple epochs until convergence.

The end-to-end performance of SGD can be measured as the time that it takes to achieve the target loss. This can be further decomposed into two metrics [95] that we will use throughout this paper. *Hardware efficiency* measures the time that SGD requires to finish one epoch. *Statistical efficiency* represents the number of epochs that SGD requires to converge.

**SGD over Low Precision Data.** Training SGD over low precision representation of the input data using a generalized linear model targets the following function:

<sup>1</sup> $\tilde{f} = 1.0$  leads to  $\tilde{a} = 2^S - 1$ .

<sup>2</sup>In this paper, three pairs of words (table, training dataset), (row, example, sample) and (column, feature) are used interchangeably.

### Algorithm 1: LOW-PRECISION SGD

**Input** :  $N$ : number of samples,  
 $E$ : number of epochs,  
 $df$ : derivative of the given loss function,  
 $\gamma$ : learning rate,  
 $Q_s(\vec{a}_i)$ :  $s$ -bit quantized data set of the  $i$ -th sample,  $\in \mathbb{F}^{1 \times M}$ ,  
 $b_i$ : label value of the  $n$ -th sample,  $b_i \in \mathbb{R}^1$ .

**Output** :  $\vec{x}$ : model with a set of parameters.

```

1 for  $e = 1$  to  $E$  do
2   for  $i = 1$  to  $N$  do
3     /* Dot product */
4     int32  $a\_dot\_x = Q_s(\vec{a}_i) \cdot \vec{x}$ ;
5     /* Serial part */
6     int32  $scale = \gamma \times df(a\_dot\_x, b_i)$ ;
7     /* Gradient computation */
8      $\vec{g} = scale \times Q_s(\vec{a}_i)$ ;
9     /* Model update */
10     $\vec{x} = \vec{x} - \vec{g}$ ;
11  end
12 end

```

$$\text{minimize}_{\vec{x}} : \frac{1}{N} \sum_{i=1}^N f(\vec{x} \cdot Q_s(\vec{a}_i), b_i),$$

where the  $i$ -th sample contains a vector of quantized  $s$ -bit values ( $Q_s(\vec{a}_i) \in \mathbb{F}^{1 \times M}$ ) and the corresponding true label value ( $b_i \in \mathbb{R}^1$ ). Algorithm 1 illustrates the control flow of low-precision SGD. SGD is iteratively evaluated in  $E$  epochs (Line 1). In each epoch, the entire low-precision training dataset is scanned, one sample per iteration (Line 2). Each sample is processed as follows. First, we compute the dot product of two vectors: the  $i$ -th low-precision sample  $Q_s(\vec{a}_i)$  and the full-precision model<sup>3</sup>  $\vec{x}$  (Line 3). Its output  $a\_dot\_x$  is a full-precision scalar value. Second, we compute the scaling value  $scale$ , based on the derivative (i.e.,  $df$ ) of the given loss function (Line 4). For different learning algorithms, we only need to modify this function to compute the scaling value, while keeping the other parts unchanged. Third, the full-precision gradient ( $\vec{g}$ ) is computed (Line 5). Fourth, the model ( $\vec{x}$ ) is updated with the calculated gradient (Line 6).

**Mini-batch SGD.** One variant of SGD that is popularly implemented in many systems is *mini-batch SGD* [55] – instead of calculating the gradient using a single sample (Line 5), mini-batch SGD uses multiple samples, called a “mini-batch”, to calculate the *average* gradient. Mini-batch SGD can be easier to accelerate because all samples in a mini-batch share the same model and thus can be processed independently in parallel. For applications such as distributed deep learning for image classification, mini-batch SGD, instead of the standard SGD, is the *de facto* training algorithm. We use mini-batch SGD in MLWeaving to address the constraints encountered when deploying SGD on an FPGA<sup>4</sup>.

## 2.3 Hardware Acceleration

Most ML algorithms are known to be compute and data intensive. Not surprisingly, in the last years we have seen a significant increase in the number of specialized hardware solutions for ML, from GPUs to FPGAs and even specialized devices such as TPUs [40]. In this paper, we focus on FPGAs since they provide a higher degree of versatility in exploring possible algorithms and designs, something important in an area that is evolving as quickly as ML. FPGAs have already been proposed as a way to accelerate a

<sup>3</sup>In this paper, we do not consider the quantization of the model.

<sup>4</sup>We explain more in Subsection 4.3.

Term	Definition	Range
$N$	Number of samples for training	Input
$M$	Number of features in the sample	Input
$B$	Batch size	Hyper-param
$\lambda$	Learning rate	Hyper-param
$s$	Number of bits used at runtime	Input
$\vec{x}$	Model, i.e., a vector of parameters	Output
$S$	Maximum number of bits of the quantized value	32
$T_s$	$s$ -bit fixed-point table (i.e., training dataset)	$1 \leq s \leq S$
$a^{[i]}$	$i$ -th bit of fixed-point value $a$ , $1 \leq i \leq S$	0 or 1
$Q_s(A)$	$s$ -bit quantized value of full-precision $A$	$1 \leq s \leq S$
$\#CL$	Number of bits of a cache line	512 bits
$\#Freq$	Frequency of the SGD hardware design	400 MHz
$\#M_{max}$	Maximum dimension of model supported	32K
$\#Bank$	Number of banks implemented in hardware	8

Table 1: Notation used in the paper

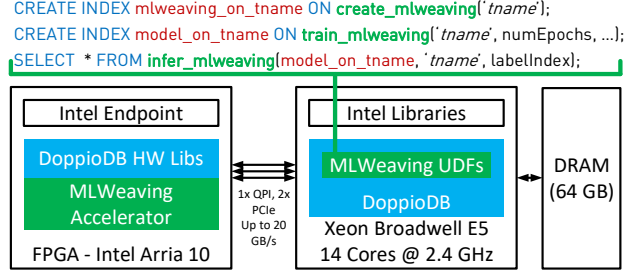


Figure 2: Target platform (Intel Xeon+FPGA Gen2), overview of DoppioDB on this platform and sample queries with MLWeaving UDFs in DoppioDB.

number of database operations [37, 39, 46, 76, 86, 87, 88] and are increasingly available, specially in cloud platforms such as Microsoft Catapult [8], Brainwave [17, 27] or Amazon F1 instances.

The degree of microarchitectural freedom in designing an algorithm is much higher on an FPGA than in software in general as it is possible to design specialized compute units from scratch and tailor the hardware to the application at hand [80]. As such, we can go beyond the von Neumann (vN) architecture with FPGAs and implement a computing task in a more elegant way. The limiting constraints in FPGA designs are *meeting timing* (how fast the hardware design can be clocked) and *resource usage* as the FPGA is a physical device and, at a certain point, there are no more gates available to implement additional logic. Often, designs balance one against the other and strive for an efficient trade-off between parallelism on the one hand and resource usage on the other hand.

## 3. SYSTEM OVERVIEW

**Target Platform.** The target platform (Figure 2) for this work is the 2nd version Intel Xeon+FPGA, combining a Broadwell 14-core CPU E5-2680v4 with an Arria 10 FPGA. The FPGA has cache-coherent access to the main memory (DDR4: 64GB) of the CPU via 1 QPI and 2 PCIe links, resulting in around 20 GB/s combined read and write bandwidth. We perform all our experiments on this machine.

**Database Integration.** We integrate our FPGA-accelerated training designs into DoppioDB [77], an open source solution for FPGA-accelerated databases, based on MonetDB [35]. DoppioDB enables easy integration of FPGA-based accelerators through a set of software and hardware libraries [66]. The hardware libraries expose a native memory interface which the FPGA accelerators use to access the main memory of the host CPU. On the software side, FPGA accelerators can be started and monitored as separate threads. These FPGA threads run in parallel to software threads.

We implement three User Defined Functions (UDF) in DoppioDB, as shown in Figure 2: (1) The first UDF is to initiate the

creation of the MLWeaving data structure. This data structure is kept internal in the database, similar to an index, associated with a certain table. (2) The second UDF is to initiate training using MLWeaving. Under the hood, DoppioDB will look for the MLWeaving index that belongs to the table given by this UDF. If found, the FPGA thread is started. It uses MLWeaving index to train a model which then gets transferred to the main memory. (3) The third UDF is to perform inference on tuples using the model that has been trained before. Similar to the MLWeaving index, the trained model is also associated with a certain table and will check during query execution if inference can be performed, conditioned on a model having been trained before.

MLWeaving combined with DoppioDB offers users a SQL front-end for learning models from relational data in a seamless manner as the data selection and transformation needed for the learning can be done using SQL and without incurring expensive data transfers in and out of the database.

## 4. MLWEAVING DESIGN

### 4.1 Design Methodology

MLWeaving involves many aspects that interact in a tight manner. To make it easier to understand how it works, we develop MLWeaving in three stages, each one with a design addressing a particular issue: “Quantized” [44], “BWeaving” (Subsection 4.2) and “MLWeaving” (Subsection 4.3), as illustrated in Table 2. Understanding of MLWeaving, requires to understand the interplay between the data representation and the processing required by the accelerator. In the case of SGD, the most important components in the design are the computing circuits and how the input data is transferred from the external memory (DRAM on the CPU socket) and how the model is accessed on the FPGA’s local memory.

**Computing Circuits.** The first design, “Quantized”, employs fixed circuits for each precision level. It, thus, requires the data to be available at the corresponding precision. “Quantized” processes features using fixed-point bit-parallel multipliers. The other two designs, “BWeaving” and “MLWeaving” use bit-serial multipliers [92], enabling on-the-fly precision selection. “Quantized” can support one precision level while both “BWeaving” and “MLWeaving” can support 32 levels.

**Memory Layouts.** In the Xeon+FPGA platform [66] used to implement MLWeaving, the FPGA has cache coherent access to the main memory of the CPU. The data arrives to the FPGA in the form of cache lines,  $\#CL$  (512 bits per cache line). Efficiency is achieved by processing in parallel as many elements within that cache line as possible. How many elements are within a cache line depends on how the data is stored in memory. “Quantized” stores each data point at a given precision in a consecutive manner. If the precision is 16 bits, every cache line brings in 512/16 dimensions (e.g., features or columns) to be processed. Because the value for each dimension arrives as a whole, the multipliers needed for the gradient computation are based on the 16-bits used to represent a value. Such 16-bit wide multipliers are complex and take up significant space. In “BWeaving” and “MLWeaving”, the data points are represented in memory not as a sequence of values but as an interwoven sequence of bits from different data points. Reading, e.g., a cache line brings in the first bit of 512 dimensions. Thus, the gradient for a data point cannot be computed right away. Instead, we use a bit-serial multiplier, where the required multiplication is performed one bit at a time with the result accumulated and added to the next one-bit multiplication until the whole multiplication for a data point is completed. With this design, “BWeaving” and “MLWeaving”

Hardware Metrics	Quantized	BWeaving	MLWeaving
Supported precision levels	$s$ -bit only	1-32	1-32
Required memory layouts	One for $s$ -bit	Shared	Shared
Bitwidth (bits) of model $\vec{x}$	$\lfloor \frac{512}{s} \rfloor \times 32$	16K	2K
Number of banks, $\#Bank$	1	1	8
Mini-batch size, $B$	$n$	$n$	$8*n$

Table 2: Comparison of three approaches.  $\#CL$  is 512 and  $\#Bank$  is 8.

use one memory layout to support arbitrary-precision data retrieving from memory, while “Quantized” requires one memory layout for each precision level.

**Accessing the Model on FPGAs.** The dot product in SGD involves not only the input data but also the corresponding entry in the model. Thus, an additional factor in the design is how to efficiently access the corresponding values of the model. A design that operates over complete values for each dimension needs to read the values from the model also as a whole. This is referred to the *bitwidth of the model*. The bitwidth is a very important parameter in an FPGA design because it affects the complexity of the interconnects and the way data has to move from the model storage to the computing units. The higher the bitwidth, the more complex the design and, thus, the higher probability that it will not meet timing at higher clock rates.

“Quantized” processes dimensions as a whole, so it has a model bitwidth of  $\lfloor \frac{512}{s} \rfloor \times 32$ , where the precision of the model is 32 bits and  $s$  is the precision level of input data. “BWeaving” has a high model bitwidth of 16K ( $32*512$ )<sup>5</sup>, making it unsuitable in real settings. “MLWeaving” reduces the bitwidth of the model by using a mini-batch SGD algorithm (Subsection 2.2) where each mini-batch is processed without modifying the model. This allows MLWeaving to adopt a multiple-bank hardware design (similar to data partitioning but in hardware) such that each bank can accommodate a sample. The hardware design of MLWeaving has 8 banks, each bank only needs to consume 64 bits to achieve the necessary throughput, 512 bits per cycle in the interwoven representation. Since all the banks share the same model, the model bitwidth becomes 2K, significantly smaller than 16K of “BWeaving” which literally uses only one bank. MLWeaving can only support a mini-batch size,  $B$ , that must be a multiple of 8. The other two designs work with any positive integer size.

### 4.2 BWeaving

We present BWeaving, which achieves the objective that both memory access and computation time scales linearly with the number of bits used for low-precision ML. BWeaving contains its own memory layout and arithmetic.

#### 4.2.1 BWeaving Memory Layout (Software)

The BWeaving memory layout is based on ideas proposed by BitWeaving [57,58]. In a nutshell, we transpose the training dataset to allow the run time selection of the level of precision and to reduce memory traffic for lower precision levels. Contrary to BitWeaving, which performs the weaving on one column, BWeaving transposes each row (a sample) to preserve access locality, since the training dataset is accessed by SGD in a *sample-at-a-time* manner.

The transposition of the data used in BWeaving is shown in Figure 3.  $M$   $S$ -bit features of a sample are transposed into  $S$   $M$ -bit

<sup>5</sup>In Intel Arria 10 FPGA [36], the model is implemented with 20-Kb memory blocks (i.e., M20Ks). Each M20K can provide a 32-bit width with ECC (or 40-bit without ECC) for the model, so a 16K-bit width requires 512 M20Ks with ECC (or 410 without ECC). It is extremely difficult to access 410 M20Ks in a lock-step manner (e.g., sharing the same read/write address) while maintaining high frequency, as M20Ks are uniformly distributed inside an FPGA.

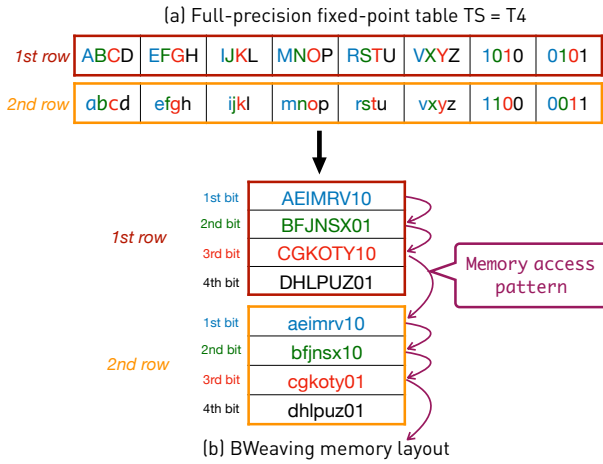


Figure 3: Full-precision fixed-point memory layout (a) converted into the BWeaving memory layout (b). Each symbol (e.g., A-Z, a-z) in the table is binary, 0 or 1. The BWeaving memory layout enables the flexible selection of precision in memory. As an example, we show the “memory access pattern” with a 3-bit precision ( $s = 3$ ).

Description	Index	Content (#CL=512 bits)
First 512 features of the first sample	0	0.511:0.0
	1	0.511:0.1
	2	0.511:0.2
	3	0.511:0.3
	...	...
Second 512 features of the first sample	32	0.1023:512.0
	33	0.1023:512.1
	34	0.1023:512.2
	...	...
	...	...
First 512 features of the second sample	128	1.511:0.0
	129	1.511:0.1
	...	...
	...	...
	...	...

Table 3: Instantiation of BWeaving memory layout.  $x_y:z_w$  denotes the  $w$ -th bits of 512 features (from  $z$ -th to  $y$ -th) in the  $x$ -th sample.

words (where  $M$  is 8 and  $S$  is 4 in the example shown). Inside the first row, eight 4-bit features are transposed into four 8-bit words. The first bits (i.e., AEIMRV10) of the first sample are stored in a 8-bit word. The second word BFJNSX01, which contains the second bits, is stored next to the first word, and so on. Between rows, the second row is stored consecutively to the first row.

Under the BWeaving memory layout, data at any level of precision can be retrieved by following a different access pattern over the same data structure. In Figure 3(b), we show the accesses needed to retrieve the data set at a precision of 3 bits. The first bits in the first row are accessed, followed by the second and third bits. Then, the access jumps to the first bits of the second row, skipping the fourth bits of each row.

**Instantiation of Memory Layout.** Table 3 shows an example of a BWeaving memory layout with  $\#CL = 512$  and  $M$  (number of features) = 2048. For instance, the first memory slot (with index = 0) is populated with the first bits of the first 512 features of the first sample, while the second memory slot (with index = 1) is populated with the second bits of the first 512 features of the first sample. If  $M$  is not a multiple of 512, we use padding to fit a 512-bit boundary.

#### 4.2.2 BWeaving Arithmetic (Hardware)

Using a bit-serial multiplier operating on the data one bit per cycle [42, 63, 78, 83, 92, 93], we design the BWeaving arithmetic

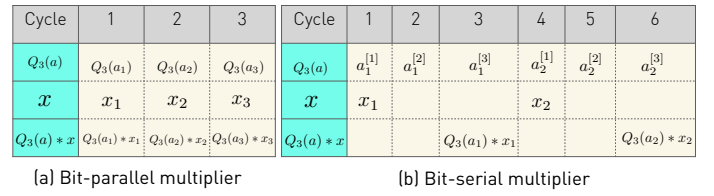


Figure 4: Multipliers: bit-parallel (a) vs. bit-serial (b). Bit-parallel multiplier produces one multiplication result per cycle, while bit-serial multiplier produces every three cycles, e.g., on cycle 3 or 6.

which provides bit-level flexibility (i.e., supporting any precision with a single hardware design) while maintaining a processing rate of a cache line per clock cycle. We now present the difference between bit-serial and bit-parallel multipliers, followed by the SGD arithmetic powered by bit-serial multiplier.

**Bit-serial Multiplier vs. Bit-parallel Multiplier.** We illustrate the difference between a bit-parallel multiplier and a bit-serial multiplier with one example multiplying 3-bit  $Q_3(a)$  (low-precision) by 4-bit  $x$  (full-precision) (Figure 4).

In a bit-parallel multiplier, each clock cycle can enable the multiplication of two numbers, in this case the quantized input  $Q_3(a)$  and the corresponding value from the model  $x$  (Figure 4a). This is the type of multiplier used in conventional CPUs and also previous specialized hardware solutions [44].

In a bit-serial multiplier, one multiplication result is produced every three cycles, a bit of  $Q_3(a)$  per cycle. After  $Q_3(a)$  is replaced with  $\sum_{i=1}^3 a^{[i]} \times 2^{-i}$  in Equation ??, the product  $Q_3(a) \times x$  in Equation (3) is computed to be the sum of the product of  $a^{[i]}$  and  $(x \ggg i)$ , where the binary value  $a^{[i]}$  represents the  $i$ -th bit of  $a$  (0 or 1),  $\ggg$  means the signed right shift, and  $i$  is from 1 to 3.

$$Q_3(a) \times x = x \times \sum_{i=1}^3 a^{[i]} \times 2^{-i} = \sum_{i=1}^3 a^{[i]} \times (x \ggg i) \quad (3)$$

In terms of cycles, the product  $Q_3(a) \times x$  is set to be  $a^{[1]} \times (x \ggg 1)$  on the first cycle,  $a^{[2]} \times (x \ggg 2)$  is added to the product on the second cycle, and  $a^{[3]} \times (x \ggg 3)$  is added on the third cycle. The advantage of bit-serial multiplier is that shift-and-add operations are enough for the calculation, considerably simplifying the design. The disadvantage is that more cycles are needed to complete the operation.

**Hardware Design of BWeaving.** The goal of BWeaving arithmetic is to consume 512-bit data per cycle from the BWeaving memory layout described above. We implement the fully-pipelined hardware design for the BWeaving arithmetic in Figure 5, according to Algorithm 1. The arithmetic has four stages, each of which occupies unique hardware resources of an FPGA. In the following, we discuss the detailed implementation for each stage.

In the “dot product” stage, 512 bit-serial multipliers are instantiated (1) to consume the 512-bit data stream (A) from the BWeaving memory layout per cycle, where each bit-serial multiplier can handle a bit from a feature per cycle. At the same time, the data stream is also fed to the “FIFO” (B). On the first cycle, the first bits from the first 512 features from a sample enter the pipeline in a lock-step manner, and 512 values are read from the *architectural model* (labelled  $\vec{x}$  in Figure 5), where the architectural model stores the committed state of the model  $\vec{x}$  to preserve the semantics of mini-batch SGD. After processing  $s$  bits of the first 512 features (where  $s$  is the precision level used in the execution), 512 multiplication results are passed to the fully-pipelined adder tree (2), whose depth is  $\log_2(512)$ . The output of the adder tree is connected to an accumulator (3), which aggregates  $\lceil \frac{M}{512} \rceil$  valid results from



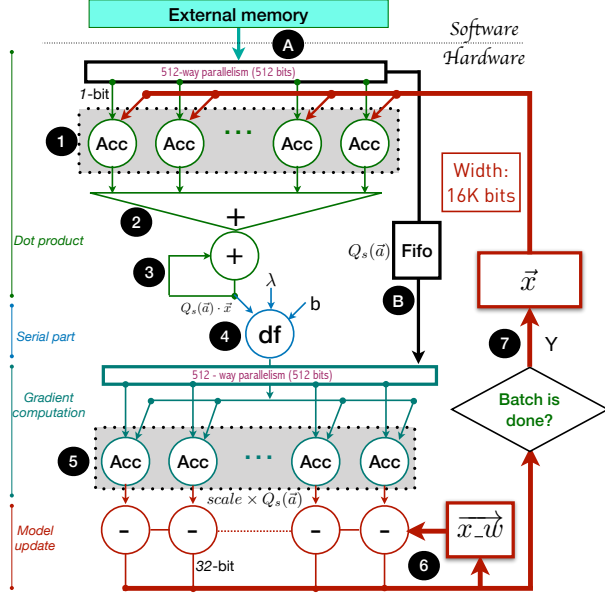


Figure 5: Hardware design of BWeaving: fully pipelined according to Algorithm 1.

the adder tree and then computes the final result  $(Q_s(\vec{a}) \cdot \vec{x})$  of the dot product<sup>6</sup>, where  $M$  is number of features in the sample.

In the “serial part” stage, the scaling value  $scale$  (4) is computed to be  $\lambda \times df(Q_s(\vec{a}) \cdot \vec{x}, b)$ , where  $\lambda$  is the learning rate (parameterizable at runtime),  $df$  is the derivative of the given loss function, and  $b$  is the label<sup>7</sup> of the sample.

In the “gradient computation” stage, we again instantiate 512 bit-serial multipliers (5) to compute the full-precision gradient with comparable throughput to the “dot product” stage. The scaling value  $scale$  is broadcast to each bit-serial multiplier as its bit-parallel input, while the bit-serial input  $Q_s(\vec{a})$  can be read from the “FIFO” (B). The bit-serial multipliers in this stage require exactly the same bit stream order of  $Q_s(\vec{a})$  as that in the “dot product” stage.

In the “model update” stage, the part of the gradient from the first 512 features is computed after  $s$  cycles, and then used to update the *working model* ( $\vec{x}_w$ ). The working model keeps the temporary model updated after each data sample is processed (6)<sup>8</sup>. Later,  $\vec{x}_w$  is updated with the part of gradient from the second 512 features after next  $s$  cycles, and so on.  $\vec{x}_w$  is updated at the rate of every sample, while the architectural model ( $\vec{x}$ ) is updated only after a mini batch ( $B$ ) of samples (7), where  $B$  is the mini batch size (parameterizable at runtime). Therefore, the semantics of mini-batch SGD is preserved.

### 4.3 MLWeaving

MLWeaving develops the ideas behind BWeaving so as to make them implementable. In particular, MLWeaving changes both the

<sup>6</sup>In the actual implementation, we adopt the distributed arithmetic computation approach [42, 92] to compute the dot product, since it produces the same result with fewer hardware resources. In the paper, we use the basic bit-serial multiplier for ease of understanding.

<sup>7</sup>In our actual implementation, we also load the label  $b$  from memory. However, we omit the related data path in Figure 5 for clarity.

<sup>8</sup>The pair (architectural model, working model) is only used in the hardware design (Figures 5, 6), analogous to the pair (architectural register, physical register) in computer architecture. The architectural register indicates the register specified by instruction set architecture (ISA), visible to the programmer. The physical register is used to store temporary results, invisible to the programmer.

### Algorithm 2: MINI-BATCH SGD UNDER MLWEAVING

```

Input :  $N$ : number of samples,
         $\gamma$ : learning rate,
         $Q_s(\vec{a}_i)$ :  $s$ -bit quantized data set of the  $i$ -th sample,  $\in \mathbb{R}^{1 \times M}$ ,
         $b_i$ : label value of the  $n$ -th sample,  $b_i \in \mathbb{R}^1$ .

Output :  $\vec{x}$ : model with a set of parameters.

1 for ( $i = 0; i < N; i += B$ ) do
2    $\vec{g} = 0$ ;
3   for ( $j = 0; j < B; j += \#Bank$ ) do
4     /* 1: Multi-bank processing */
5     #pragma parallel in hardware
6     for ( $k = 0; k < \#Bank; k ++$ ) do
7       int32  $t = i + j + k$ ;
8       /* 1.1: Dot product */
9       int32  $a\_dot\_x = Q_s(\vec{a}_t) \cdot \vec{x}$ ;
10      /* 1.2: Serial part */
11      int32  $scale = \gamma \times df(a\_dot\_x, b_{i+j+k})$ ;
12      /* 1.3: Gradient computation */
13       $g_{j+k} = scale \times Q_s(\vec{a}_t)$ ;
14      /* 2: Gradient accumulation */
15       $\vec{g} = \vec{g} + g_{j+k}$ ;
16   end
17   /* 3: Model update */
18    $\vec{x} = \vec{x} - \vec{g}$ ;
19 end

```

memory layout and the design on the FPGA to dramatically reduce the required bitwidth of the model. Inspired by mini-batch SGD which uses the same model to process one mini batch of  $B$  samples, we can process multiple samples in the same mini-batch simultaneously such that we can reduce the model bitwidth without compromising on throughput: 512 bits per cycle. As shown in Algorithm 2, MLWeaving instantiates 8 physical banks to accommodate 8 samples in the same mini-batch simultaneously (Line 4) such that 8 samples reading the same portion of the model are processed in a lock-step manner. This is why  $B$  must be a multiple of 8. Meanwhile, we also adjust the related memory layout such that the data stream from the memory flows into the MLWeaving hardware without any transposition overhead.

#### 4.3.1 MLWeaving Memory Layout (Software)

Starting from the BWeaving memory layout in Figure 3, we show the memory layout transition to MLWeaving in Figure 7. BWeaving populates each memory transaction with eight bits from the same row, e.g., **AEIMRV10** of the first row. In contrast, the first/second row contributes four bits for each memory transaction under MLWeaving. For instance, the first bits of the first four features of two rows assemble into the first memory transaction, e.g., **AEIMaeim**. Since the bits **AEIM** and **aeim** share the same weights, the model only needs to provide four weights within a cycle.

**Instantiation of Memory Layout.** We instantiate the MLWeaving memory layout by setting  $\#CL$  (or  $\#Bank$ ) to be 512 (or 8). Now we use the case with  $M = 2048$  as an example in Table 4. For instance, the first memory transaction is populated with the first bits of the first 64 features of the first eight samples. If  $M$  is not a multiple of 64, we use padding to align it to 64 bits. Thus, the memory traffic  $MT$  (in terms of bits) for each sample consists of two parts, as shown in Equation 4. The first part indicates the memory traffic from all the features, evaluated to be the precision level  $s$  multiplied by the value that rounds up  $M$  to the nearest multiple of 64. The second part (32 bits) comes from the label of each sample.

$$MT = s \times \lceil \frac{M}{64} \rceil \times 64 + 32 \quad (4)$$

#### 4.3.2 MLWeaving Arithmetic (Hardware)

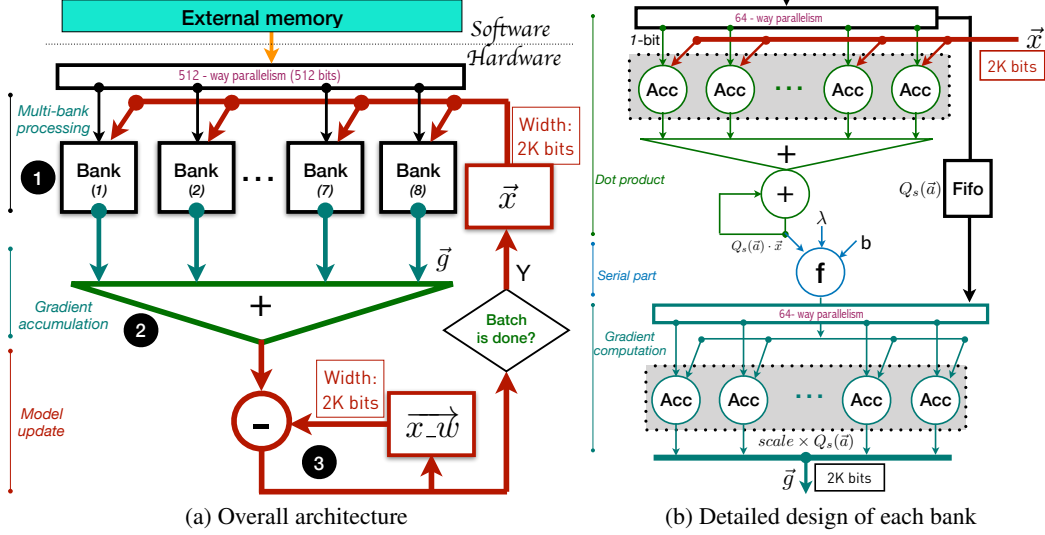


Figure 6: Fully pipelined MLWeaving arithmetic with 8 banks, according to Algorithm 2. Its throughput is 512 bits per cycle.

Description	Index	Bank 7	...	Bank 1	Bank 0
First 64 features of the first 8 samples	0	7.63:0.0	...	1.63:0.0	0.63:0.0
	1	7.63:0.1	...	1.63:0.1	0.63:0.1
	2	7.63:0.2	...	1.63:0.2	0.63:0.2
	31	7.63:0.31	...	1.63:0.31	0.63:0.31
Second 64 features of the first 8 samples	32	7.127:64.0	...	1.127:64.0	0.127:64.0
	...	...	...	...	...
First 64 features of the second 8 samples	1024	15.63:0.0	...	9.63:0.0	8.63:0.0
	...	...	...	...	...

Table 4: Instantiation of MLWeaving memory layout.  $x.y.z.w$  denotes the  $w$ -th bits of 64 features (from  $z$ -th to  $y$ -th) in the  $x$ -th sample and  $y - z = 63$ . A row contains a cache line (512 bits).

Name	Logic (ALMs)	DSPs	BRAMs	Frequency
BWeaving	N.A	N.A	N.A	N.A
MLWeaving	35670 (8.4%)	0 (0%)	3.25Mb (6.1%)	400 MHz

Table 5: Resource consumption

Following Algorithm 2, we present the fully-pipelined hardware design of MLWeaving arithmetic in Figure 6. The targeted throughput of MLWeaving arithmetic is 512 bits per cycle. It consists of three main pipeline stages. In the following, we explain the design details of each pipeline stage.

In the “multi-bank processing” stage, the 512-bit computing pipeline is divided into 8 banks, each of which consumes 64 bits from one sample (1), as shown in Figure 6a. The most important property of this stage is that 8 banks read the same portion of model at a time. Each bank behaves the same as that in the BWeaving arithmetic in Figure 5, except that each bank instantiates 64 bit-serial multipliers in the “dot product” and “gradient computation” stages. Since we instantiate 8 banks, the total throughput of the MLWeaving arithmetic is still 512 bits per cycle.

In the “gradient accumulation” stage, a portion of gradient (64 32-bit elements) from 8 banks is fed to 64 element-wise adder trees, each of which generates one element of the accumulated gradient (2). In the “model update” stage, the accumulated gradient is used to update the working model ( $\vec{x} \cdot \vec{w}$ ) (3) for every 8 samples. Mean-

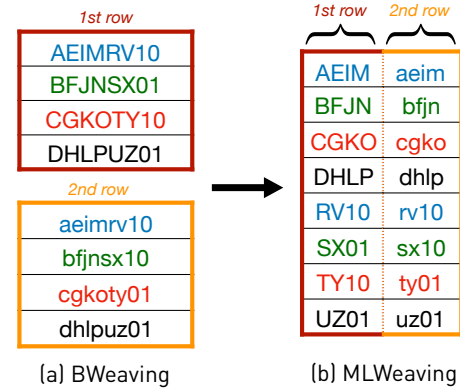


Figure 7: BWeaving memory layout (a) converted to MLWeaving memory layout (b):  $\#CL = 8$ ,  $\#Bank = 2$  and  $M = 8$ .

while, the architectural model ( $\vec{x}$ ) is updated only after a mini batch ( $B$ ) of samples.

**Instantiation of hardware design.** Table 5 shows the resource consumption in our FPGA when implementing the computing pipeline in MLWeaving. MLWeaving achieves high clock frequency (400MHz) while requiring a reasonable amount of FPGA resources. This is because 1) the proposed multi-bank architecture of MLWeaving leads to fewer BRAMs (on-chip memory blocks on FPGAs) for the architectural and working models in Figure 6, and 2) the memory layout allows MLWeaving to directly consume data from memory, without auxiliary hardware modules for transposition. The theoretical throughput of MLWeaving’s hardware design is roughly 25.6GB/s (400M \* 512 bits per cycle), much larger than the available memory bandwidth: 15GB/s.

## 5. PRESERVATION OF PRECEDENCE

We propose a simple yet efficient scheme to keep SGD hardware design synchronous, without compromising computation speed. Our scheme is orthogonal to the BWeaving and MLWeaving designs, so

it can be applied to both<sup>9</sup>. We first identify the performance issues of synchronous SGD, and then describe our scheme.

According to Algorithm 2, model reading (Line 7) and model updating (Line 13) has a RAW (Read After Write) dependency, due to the inherently sequential nature of synchronous SGD. For example, the model read by the second batch ( $B$  samples) should be up-to-date such that the gradient from the first batch has already been accumulated into the model, as shown in Figure 8a. In other words, the second batch has to wait until the model is updated. In particular, it takes  $\lceil M/64 \rceil * s$  cycles to update the model, where  $M$  is the number of features, 64 is the number of elements written to the model within a cycle, and  $s$  is the number of cycles to do one multiplication with the bit-serial multiplier.

We aim to preserve the dependency and improve the performance of the synchronous SGD design. Our aim is three-fold. First, it lets SGD read the up-to-date model. Second, it can support various batch sizes ( $B$ ). Third, it explores the greatest possible overlap between computation (i.e., dot product) and communication (i.e., model update). The first two requirements are to preserve the precedence for synchronous SGD, so we propose a basic scheme to meet them. The third requirement is to maximize performance, we address it separately using a chaining-enhanced approach.

**Basic Mechanism.** The basic synchronous design only requires the maintenance of two 16-bit registers: *wr\_counter* and *rd\_counter*. Table 6 demonstrates the basic mechanism to meet the first two requirements. In the following, we describe how to use these two counters to preserve the dependency.

The *wr\_counter* records the counter for the writing side of the model  $\vec{x}$  in the “model update” stage. Its initialization value is  $B$ , where  $B$  is input batch size. It means that  $B$  credits are provided at the beginning for  $B$  samples to read  $\vec{x}$  in the “dot product” stage. *wr\_counter* is incremented by  $B$  when the model is updated, indicating that  $\vec{x}$  is updated by the aggregated gradient from every  $B$  samples in Algorithm 2. We can update the *wr\_counter* once the aggregated gradient is ready, since there is no WAR or WAW dependency.

The *rd\_counter* records the counter for the reading side of the model  $\vec{x}$  in the “dot product” stage. Its initialization value is 0, indicating that  $\vec{x}$  has not been read yet. It is incremented by 8 when the model is read, since MLWeaving processes 8 samples concurrently. Its updating condition is that *rd\_counter* is not equal to *wr\_counter*, indicating there are still enough credits for samples to read  $\vec{x}$ . This is the critical step to preserve the dependency.

**Chaining-enhanced Mechanism.** In order to tolerate the long pipeline latency when updating the model, we propose the chaining-enhanced mechanism for synchronous SGD. We treat the model  $\vec{x}$  as a vector register, which requires multiple cycles to read/write and follows a sequential access pattern. Then, we use the chaining technique [24, 50, 51, 72] of vector processing to maximally overlap the computation and model updating. In particular, the model updated with the gradient from the first batch can be forwarded to the second batch before the entire updating operation completes, as shown in Figure 8b. The second batch can begin to read after  $s$  cycles, where  $s$  is the precision level. We observe that it is safe for the second batch to read the model after the first part of model (e.g., 64 values) is updated into the model. The data dependency is preserved since the model updating speed is not slower than the model reading speed.

## 6. PER-EPOCH TUNING OF PRECISION

<sup>9</sup>In the following, we mainly describe our scheme for MLWeaving. Actually, we can easily generalize to BWeaving.

	Init Value	Step Size	Updating Condition
<i>wr_counter</i>	$B$	$B$	Always ok
<i>rd_counter</i>	0	8	$rd\_counter \neq wr\_counter$

Table 6: Basic mechanism to resolve RAW hazard for MLWeaving

MLWeaving introduces one tuning knob for the user: *the precision level to be used for training*. Most existing work assumes that it is the user’s responsibility to set the right precision level. This is understandable as the right level depends on both the data and the error tolerance with no tight theory to map error tolerance back to the precision level.

In this paper, we do not address the problem of mapping precision and error levels as it goes well beyond the scope of the work. Instead, we provide a simple, dynamic schedule of precision that works robustly on all data sets we have and illustrates the potential of MLweaving for supporting dynamic precision scheduling.

**Dynamic Precision Schedule.** Our schedule is based on a very simple observation — at the beginning of the training, the system is less sensitive to the error introduced by low precision data representation; at the end of the training, the system often requires more bits to converge. MLWeaving allows us to dynamically change the number of bits to use for each epoch. We exploit this flexibility and build a simple dynamic precision schedule: use 2 bits for the 1st-4th epochs, 3 bits for the 5th-8th epochs, 4 bits for the 9th-16th epochs, 5 bits for the 17th-32nd epochs, and so on. That is, the number of bits grows over time until we reach the targeted loss.

This simple schedule is inspired by the following theoretical observation — for SGD to converge with  $O(1/\sqrt{K})$  rate, at each iteration  $K$ , it only requires that the bias introduced by the low precision representation decreases faster than  $O(1/K)$ . The above schedule is one example that satisfies this property, as the bias introduced by low precision is halved when one more bit is used.

**Remarks.** Note that the above schedule is far from optimal and perfect — One can design more adaptive schedules by, for example, monitoring the speed of the decrease of loss and dynamically choosing when to switch to the next level of precision. MLWeaving allows this possibility by providing an end-to-end solution that enables dynamic precision scheduling. We will explore more sophisticated precision scheduling schemes as well as the problem of mapping precision and error levels as part of future work.

## 7. EXPERIMENTAL EVALUATION

### 7.1 Experimental Setup

**Workloads.** We carry out our experiments with the five data sets shown in Table 7. For the multi-class dataset TL [45], we use 10 classes of ImageNet. Instead of directly using the images in ImageNet, we use 2048 features per sample extracted by a neural network (InceptionV3) that can be used for transfer learning, and we train binary classifiers using the one-vs-one strategy. For the dataset Madelon, the training samples are duplicated 10 times so that the size exceeds the capacity of the last level cache in the CPU. For the dataset KDD, since its original dataset is highly skewed, i.e., 93% samples labelled 0, we uniformly delete the samples labelled 0 so that the final dataset is balanced.

**CPU Baselines.** Since SGD is inherently sequential, keeping consistency when running SGD leads to no parallelism among cores. Two variants of SGD (“Hogwild” and “ModelAverage”) have been proposed to parallelize SGD on modern CPUs and we use both as baselines, employing existing optimization methods, e.g., multi-threaded (14 cores), low-precision (8-bit) and AVX2 instructions.

“Hogwild” [70, 95] allows each thread (i.e., core) to compute the gradient from its own portion of dataset and then to perform asynchronous update on a single copy of the model without any syn-



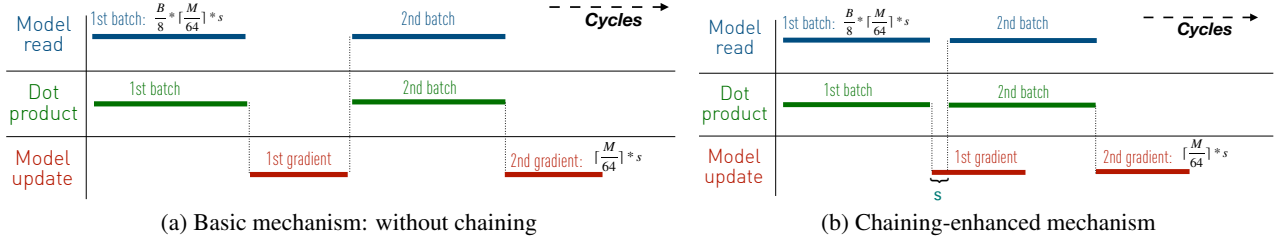


Figure 8: MLWeaving with and without chaining.

chronization. Therefore, the parallelism among cores is exploited at the cost of noise from asynchronous updates. Even though no synchronization is required, Hogwild still suffers from severe cache coherence overhead, i.e., invalidating the potential copy of model in the private caches of other cores before the real write operation. The cache coherence overhead is so severe on a multi-core CPU that Hogwild cannot benefit from using low-precision, as shown in Figure 15b.

“ModelAverage” [97] allows each thread to have its own copy of the model so that no costly invalidation among cores occurs. It averages the models at the end of each epoch and then broadcasts the aggregated model to each thread at the beginning of next epoch. Therefore, its multi-threaded implementation can reach the maximum memory bandwidth of the CPU (leading to high hardware efficiency). However, ModelAverage has relatively lower statistical efficiency since each worker uses its local (not global) model to compute the gradient. Since its 32-bit floating-point implementation is memory-bound, ModelAverage can significantly benefit from low-precision dataset which requires less memory traffic. In our experiment, we choose 8-bit precision because 1) the smallest bank width of a SIMD register is 8 bits and 2) ModelAverage becomes compute-bound when the dataset is quantized to 8 bits, indicating lower performance for a lower-than-8-bit precision.

**Learning Rate Schedules.** During training, the learning rate decays based on a pre-defined schedule to achieve higher convergence rate. We describe our concrete learning rate schedules on FPGAs and CPUs. On CPUs, the schedule determines the learning rate ( $\lambda_e$ ) of the  $e$ -th epoch to be  $\lambda \times \beta^{\sqrt{e}}$ , where  $\lambda$  is the initial learning rate while  $\beta$  is the decay factor. In our experiment, more aggressive decay policy, e.g.,  $\lambda/\sqrt{e}$  or  $\lambda/e$ , slows down the convergence rate. We find that a constant learning rate leads to the best performance for several datasets. On FPGAs, we employ a relatively simple schedule, as shown in Equation 5, where  $\alpha$  is the threshold to decay the learning rate, because 1), on FPGAs, we apply the learning rate ( $\lambda_e$ ) as a right-shift operator and then  $\lambda_e = 2^{-j}$ , where  $j$  is an integer; and 2) MLWeaving (sync) needs a lower number of epochs to converge to the same training loss than its CPU rivals (not sync).

$$\lambda_e = \begin{cases} \lambda, & e \leq \alpha \\ \lambda * 0.5, & e > \alpha \end{cases} \quad (5)$$

**Comparison Methodology.** Our evaluations mainly validate three hypotheses. First, MLWeaving can achieve linear speedup when a smaller number of bits is used in the training (Subsection 7.2). Second, MLWeaving can converge faster than its CPU counterparts (Subsection 7.4). Third, the dynamic precision scheduling can further accelerate the convergence process (Subsection 7.5).

## 7.2 Hardware Efficiency: Time of Each Epoch

In this subsection, we demonstrate the hardware efficiency of MLWeaving, i.e., elapsed time for each epoch. Our objective is two-fold. First, we analyze the performance characteristics of ML-

Dataset	Features	Training samples	Testing samples	Classes
Gisette [10]	5000	6000	1000	2
TL [45]	2048	26,000	5200	10
Epsilon [10]	2000	40,000	10,000	2
KDD [60]	2399	40,000	44772	2
Madelon [10]	500	20,000	600	2

Table 7: Datasets.

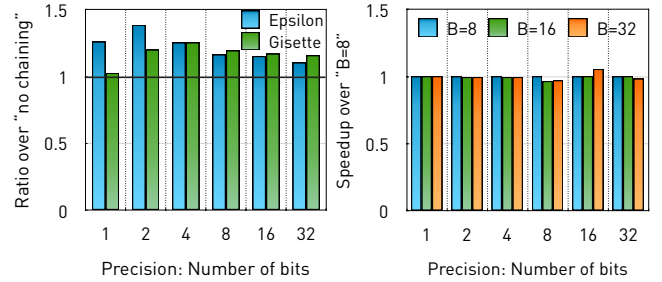


Figure 9: Effect of hardware characteristics on hardware efficiency.

Weaving<sup>10</sup> on FPGAs. Second, we compare MLWeaving with the state-of-art implementations on CPUs.

### 7.2.1 Hardware characteristics of MLWeaving

We analyze five different hardware properties of MLWeaving. In our analysis, we typically run 50 epochs and get the average time for each epoch.

**Effect of Chaining.** We examine the effect of our chaining technique (Section 5) which relaxes the unnecessary RAW dependency for MLWeaving. Figure 9a demonstrates the speedup of “chaining” over “no chaining” for two datasets. The batch size is 8. The x-axis ( $s$ ) depicts the precision  $s$ . We observe that with chaining, we can achieve up to 1.4X speedup over “no chaining” for different combinations of precision level ( $s$ ) and number of features, since “chaining” can fully overlap computation and memory access. In order to fully understand the trend, we develop an analytical cost model to predict the performance trend, as shown in Appendix. We conclude that “chaining” significantly increases the hardware efficiency.

**Effect of Mini Batch Size.** We examine the effect of mini batch size ( $B$ ) on hardware efficiency. Figure 9b illustrates the speedup of various batch sizes over “B=8” for the dataset Gisette. We observe that performance is roughly stable for different batch sizes, since MLWeaving is able to maximally overlap computation and memory access, regardless of batch size. We conclude that the batch size has a negligible effect on the hardware efficiency.

**MLWeaving (sync) vs. MLWeaving (async).** We examine the effect of the RAW dependency which is used to guarantee that SGD

<sup>10</sup>In the following experiments, by default, MLWeaving means MLWeaving (sync) on FPGAs and the chaining is enabled.

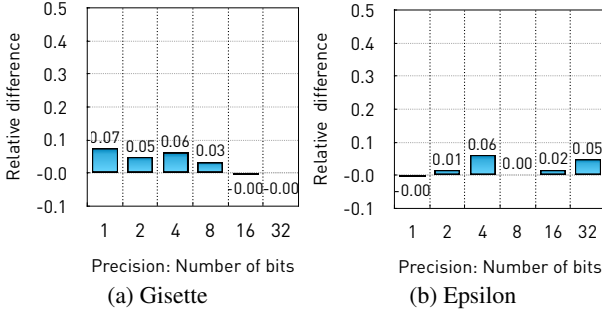


Figure 10: Relative performance difference between MLWeaving (sync) and MLWeaving (async).  $B$  is 16.  $s$  is 8.

always reads the up-to-date model, i.e., execute synchronously. If the RAW dependency is violated, SGD is executed asynchronously. Intuitively, MLWeaving (async) would be faster than MLWeaving (sync), since its computing pipeline can directly do the computation without any dependency. However, since both approaches are memory-bound on the targeted FPGA, their relative performance difference, i.e., (MLWeaving (sync) - MLWeaving (async)) / MLWeaving (sync), is small, as shown in Figure 10. We conclude that MLWeaving (sync) which preserves the RAW dependency has little effect on hardware efficiency, with the help of our chaining technique.

**Effect of Precision Level on Execution Time.** Figure 11 provides the performance improvement of various precision levels over the full-precision implementation “32-bit” under MLWeaving for two datasets. We make two observations. First, the performance of MLWeaving improves roughly linearly as bit precision reduces, especially when  $s$  is larger than 4. Second, when  $s$  is less than 4, the speedup is sub-linear since the benefit from our chaining technique cannot fully amortize the negative impact of the inherent pipeline latency. We conclude that MLWeaving can significantly reduce the elapsed time when using a smaller number of bits.

**Effect of Precision Level on Memory Traffic.** Figure 12 illustrates the memory traffic required by each sample, as  $s$  is varied. We observe that the required memory traffic almost increases linearly as the precision level increases, consistent with the trend demonstrated in Equation 4. We conclude that the MLWeaving memory layout enables an efficient data retrieval from memory for any precision level at runtime.

### 7.2.2 Comparison with CPU Implementations

We compare the performance of MLWeaving with two state-of-art CPU algorithms: “Hogwild” and “ModelAverage”, and report the result in Figure 13. Both CPU algorithms are fully optimized, they use a low-precision dataset, employ all the 14 cores and are AVX2-enhanced. “x-FP” (or “x-char”) indicates “x” with floating-point (or char) dataset, where “x” is “Hogwild” or “ModelAverage”. We use two metrics for comparison: time and memory traffic. “MLWeaving-32bit” (or “MLWeaving-8bit”) means MLWeaving with  $s = 32$  (or 8) on FPGAs.

**Time.** Figure 13a illustrates the normalized performance of two CPU approaches and MLWeaving. We can make two major observations. First, “ModelAverage-FP” is roughly 4 times faster than “MLWeaving-32bit”, since both are memory-bound and the memory bandwidth of CPU (i.e., 60GB/s) is roughly four times as much as that of FPGA (i.e., 15GB/s). “ModelAverage-FP” and “MLWeaving-8bit” roughly have the same performance, while “ModelAverage-char” which is compute-bound is obviously faster than “MLWeaving-8bit”. Second, even though “Hogwild-FP” is faster than “MLWeaving-32bit”, it is still compute-bound since it suffers from severe cache

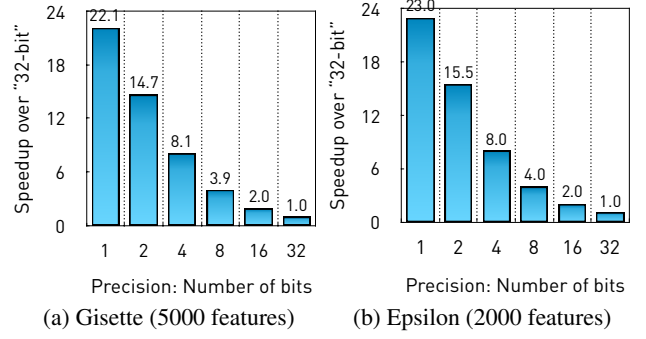


Figure 11: Relative performance increase of various precision levels over “32-bit”, where “32-bit” means the case with  $s = 32$ .

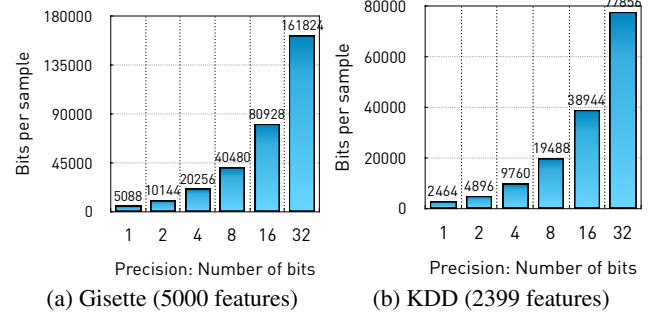


Figure 12: Memory traffic (bits) per sample as the precision varies.

coherence overhead due to the fact that multiple cores try to update the same memory address. When the model dimension becomes smaller, the overhead becomes larger as cache invalidation occurs more frequently among cores.

**Memory Traffic.** Figure 13b shows the normalized memory traffic, where the memory traffic on the CPU is collected using the Intel Performance Counter Monitor [81]. We can observe that both “Hogwild-FP” and “ModelAverage-FP” require roughly the same memory traffic as “MLWeaving-32bit”, since their datasets are all full-precision (32-bit), while “Hogwild-char” and “ModelAverage-char” require roughly the same amount of memory traffic as “MLWeaving-8bit”.

We conclude that due to the small amount of memory bandwidth available on FPGAs, MLWeaving has raw performance advantages over CPU approaches only when the chosen precision level is relatively low, e.g., less than 4.

### 7.3 Statistical Efficiency: Loss vs. Epochs

We analyze the statistical efficiency of MLWeaving. We mainly validate that MLWeaving requires significantly fewer number of

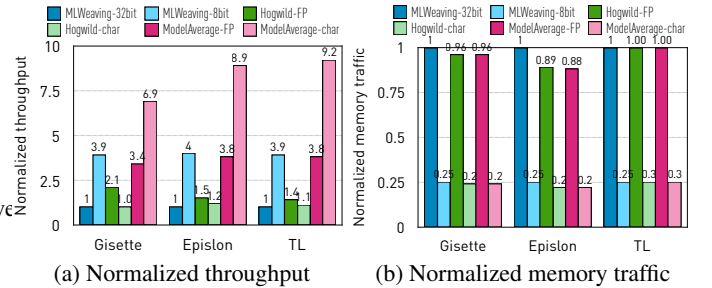


Figure 13: Hardware efficiency: MLWeaving vs. CPU rivals.

epochs to converge than its state-of-the-art CPU rivals.

**MLWeaving vs. CPUs.** We compare the statistical efficiency between MLWeaving and two full-precision CPU approaches for two datasets Epsilon and KDD<sup>11</sup>, as shown in Figures 15a, 15d. We observe that MLWeaving requires a fewer number of epochs to converge than its CPU counterparts, even though MLWeaving uses 3-bit precision and CPU approaches use full precision. For example, MLWeaving requires only 40 epochs to converge for the dataset Epsilon, while “ModelAverage” (or “Hogwild”) needs 392 (or 199) epochs to converge to the same loss in Figure 15a. The underlying reason is that MLWeaving is always working on the up-to-date model while “ModelAverage” and “Hogwild” are not.

**Impact of Mini Batch Size.** We examine the impact of batch size  $B$  on statistical efficiency under MLWeaving. Figure 14 compares the convergence trend with different batch sizes for the datasets Gisette and KDD. We run 40 epochs and observe the training loss for each epoch. We find that a larger batch size leads to a slightly slower convergence speed. Thus, we prefer to use a small mini-batch size to train for MLWeaving.

## 7.4 End-to-End Comparison: Loss vs. Time

We validate that MLWeaving outperforms its CPU rivals in terms of end-to-end performance (training loss vs. time), even though the CPU has 4 times more memory bandwidth than the FPGA. We employ two datasets Epsilon and KDD<sup>12</sup> to demonstrate the comparison result, as shown in Figures 15. We make three observations.

First, MLWeaving uses low-precision dataset to converge to the same training loss as “ModelAverage” (or “Hogwild”) works on the full-precision dataset. For example, 3-bit precision is good enough for training the dataset Epsilon, indicating great potential for low-precision training. Second, Low-precision Hogwild slightly slows down the training. Since Hogwild is bounded by cache coherence overhead, low precision, which potentially speeds up other parts of SGD, causes more cache coherence traffic among cores, as shown in Figure 15b. Third, MLWeaving requires up to 25X less memory movement to converge to the same loss, compared with its low-precision CPU counterpart, as illustrated in Figures 15c. Thus, MLWeaving could provide 25X speedup if the FPGA had comparable memory bandwidth, leading to significantly more energy-efficient training than its low-precision CPU counterparts. We conclude that MLWeaving, with the low-precision and synchronous training on FPGAs, greatly outperforms the state-of-the-art low-precision and asynchronous training on CPUs for linear model.

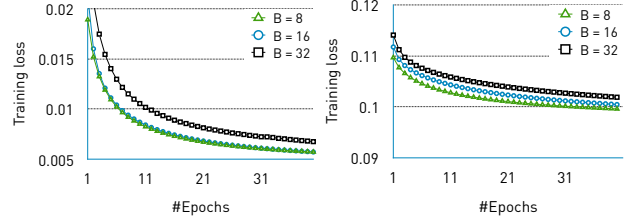
## 7.5 Effect of Flexible Precision Schedule

Table 8 shows the speedup that MLWeaving with dynamic precision scheduling achieves over MLWeaving with fixed precision and over the fastest CPU method with fixed precision. The CPU approach is fully optimized. We make two observations.

First, the dynamic precision scheduling (i.e., “adaptive” approach) reduces end-to-end training time averagely by 1.19x, compared with “non-adaptive” approach which uses fixed precision under MLWeaving. Second, the dynamic precision scheduling sometimes can lead to slowdowns, for instance for Epsilon. The reason is that Epsilon only needs 40 epochs to train with a low-precision (i.e., 3-bit) dataset to converge to the targeted loss, while our dynamic precision scheduling in Section 6 uses the precision (above 3 bits) after 8 epochs. The precision (above 3 bits) converge as fast as the

<sup>11</sup>We do not examine lower-precision (i.e., less than 8 bits) CPU approaches, as a lower precision always leads to a slightly worse statistical efficiency.

<sup>12</sup>We only put the results of two datasets with the largest and smallest speedups in Figure 15, while the results of the other datasets are in Figure 19 of Appendix.



(a) Gisette,  $\lambda = 1/2^7$

(b) KDD,  $\lambda = 1/2^8$

Figure 14: Effect of batch size on statistical efficiency.  $s$  is 8.

Adaptive Approach	TL	Gisette	KDD	Madelon	Epsilon
Vs. non-adaptive (time)	1.26×	1.5×	0.92×	1.35×	0.9×
Vs. fastest CPU (time)	10.7×	16.5×	3×	6.1×	9.9×

Table 8: End-to-end speedup thanks to flexible precision schedule.

3-bit precision while it is slower than the 3-bit precision. We conclude that the dynamic precision scheduling can reduce end-to-end training time even with a simple precision scheduling, indicating a great potential for dynamic precision scheduling.

## 8. RELATED WORK

To our knowledge, MLWeaving is the first novel solution for data representation and hardware acceleration for ML in database engines. MLWeaving builds on previous work from multiple communities: databases, machine learning, and computer architecture.

**Bulk bitwise operations.** Bulk bitwise operations [2, 26, 48, 56, 57, 58, 65, 71, 74, 89] have been used in a variety of applications, including database scans [26, 57, 58]. Among them, MLWeaving is inspired by BitWeaving [57], a transposed columnar storage layout designed for predicate evaluation on a per-column basis. BitWeaving is very efficient when answering a subfamily of relational queries. The memory layout used in MLWeaving is different from BitWeaving to accommodate the access pattern of batch SGD and the hardware implementation on an FPGA.

**FPGA-accelerated ML/DL.** MLWeaving builds on a growing line of research accelerating machine learning with FPGAs [5, 6, 9, 16, 17, 19, 27, 44, 61, 62, 64, 75]. Closest to MLWeaving is the work by De Sa et al. [19] and Kara et al. [44] using FPGAs to implement low-precision generalized linear models, and they are asynchronous. These previous methods achieve good performance using individual circuits for each level of precision. Microsoft Brainwave [17] leverages FPGA to implement low-precision programmable NPU for DNNs inference at scale. It can support four low precision levels: 8/16-bit int and ms-fp9/8. We think our MLWeaving has the great potential to apply to Brainwave to enable any-precision inference. In contrast, MLWeaving provides a single, flexible design for all precision levels without having to be redeployed on the FPGA.

**Low-Precision DNNs.** One specific application whose low precision implementation on hardware has been intensively studied is Deep Neural Networks. Prior efforts [3, 11, 20, 21, 30, 41, 42, 49] explore the fine-grained variation in bit-level precision for DNN inference, so their computation time is proportional to the bitwidth used. Since the computation time dominates the overall performance for their DNN inference, the overall performance scales linearly with the bitwidth. Other research [1, 4, 7, 12, 13, 14, 18, 22, 29, 31, 38, 40, 40, 52, 59, 69, 84, 94] has been focused on using a fixed-point, low-precision data representation and arithmetic to accelerate DNNs, instead of using full-precision. For example, TPU [40] features 64K 8-bit fixed-point MACs to accelerate neural network inference. More information about DNNs can be found in the survey [79]. Compared with these efforts, MLWeaving focuses on a

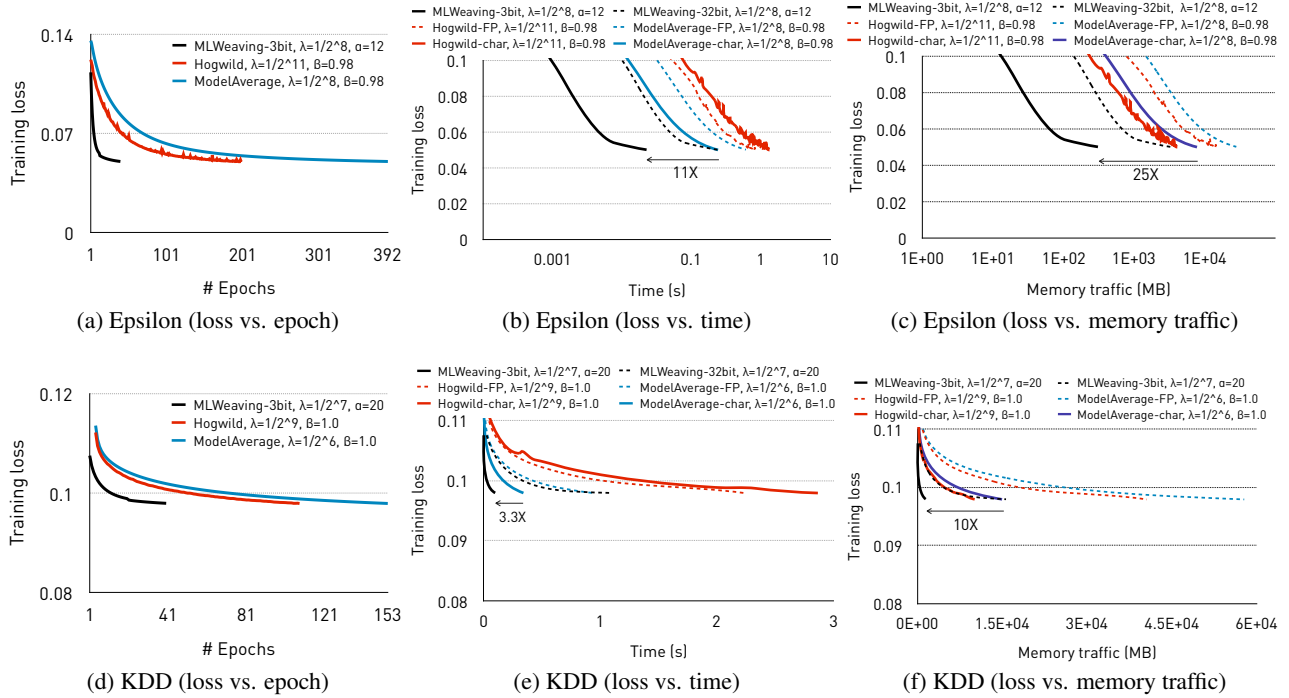


Figure 15: Convergence comparison: loss vs. epoch/time/memory traffic. The batch size is 8. Speedup indicates MLWeaving vs. fastest 14-core AVX2-enhanced low-precision CPU approach, in terms of time and memory traffic.

different workload, i.e., generalized linear model, and focuses *not* on the quantization of the *input data*, but on flexible data retrieval. As part of future work we want to investigate whether the design in MLWeaving can also be used to accelerate DNNs.

**Compression on DB/ML.** Previous work [15, 25, 28, 32, 34, 53, 65, 67, 68, 71, 73, 91] employ the compression techniques, e.g., dictionary encoding, to compress the data such that the further memory traffic can be significantly reduced at the cost of lightweight decompression overhead. Previous work [23, 47] directly performs compressed operations on sparse data representations to accelerate linear algebra. On the contrary, MLWeaving exploits the low precision of dataset to accelerate machine learning training.

## 9. CONCLUSION

MLWeaving is an innovative solution for embedding machine learning in relational engines and take advantage of modern hardware. It consists of an in-memory data storage layout that allows an efficient retrieval of quantized data at any level of precision, an efficient implementation of SGD on an FPGA, and an adaptive algorithm to learn a model using lower precision but without having to determined the level of precision in advanced. MLWeaving achieves linear speedup when decreasing the precision level and it can achieve up to a 16X performance improvement compared to the state-of-the-art low-precision first-order CPU implementation.

**Future Directions and Limitations.** The current prototype of MLWeaving has a number of limitations that will require additional work to make learning in databases of generalized linear models possible in all cases. Some of these limitations are methodological and affect the ML algorithms used. Others are a question of exploring the design space enabled by MLWeaving in more detail, which cannot be done in this paper for reasons of space. A first methodological limitation of MLWeaving is that, as is, it only supports dense, numerical data. This is fine in *some* applications as it is not uncommon for sparse and categorical values (e.g., YouTube video

IDs) to be mapped to a dense embedding. However, there are cases where training directly on sparse or categorical data is still necessary. To support the latter case, MLWeaving would need to be extended by potentially combining it not only with other lossless compression strategies but also with ML techniques such as feature hashing [90] and weight sharing [32]. A very interesting future research direction MLWeaving opens is the development of a unified data structure supporting dense, sparse, categorical, or numerical data while providing similar level of flexibility as MLWeaving.

Another methodological limitation of MLWeaving is that it currently only supports generalized linear models. However, as long as the loss function is Lipschitz continuous over the input data and the data access pattern is row-wise, it is likely that similar techniques could still be applied with some adjustments. Thus, another interesting future direction is to adapt MLWeaving to problems such as matrix factorization [54] or clustering using K-Means [43].

An area where MLWeaving needs more work is dynamic precision scheduling. The current strategy is based on a simple intuition just to illustrate the benefit provided by MLWeaving. More sophisticated dynamic schedules will require a systematic analysis of the convergence properties with the dynamic precision changes. For example, one could use a technique similar to how AdaComm [85] dynamically adjusts communication frequencies — write down the convergence upper bound with respect to the precision schedule and choose the schedule that minimizes the convergence upper bound. We leave this direction to future work.

Limitations of MLWeaving caused by the current implementation and hardware can be solved using different platforms or more complex designs. For example, MLWeaving currently supports models up to 32K dimensions due to the available on-chip memory capacity. It is reasonable to expect that the capacity will increase in future FPGAs. Also, the learning rate supported by MLWeaving can only be  $2^{-j}$ , where  $j$  is an integer, since MLWeaving uses a right-shift operator to control the learning rate. It is not clear how limiting this is in practice given the current results but we will ex-



plore different hardware designs to provide more flexibility as part of future work.

**Acknowledgments.** The presented results were partially obtained on resources hosted at the Paderborn Center for Parallel Computing (PC<sup>2</sup>) in the Intel Hardware Accelerator Research Program (HARP2). We thank Intel for their generous donation of HARP2 machine used in the work.

## 10. REFERENCES

- [1] J. M. L. T. G. P. A. Jain, A. Phanishayee. Gist: Efficient data encoding for deep neural network training. In *Proceedings of the 44th Annual International Symposium on Computer Architecture*, ISCA '18. ACM, 2018.
- [2] S. Aga, S. Jeloka, A. Subramanian, S. Narayanasamy, D. Blaauw, and R. Das. Compute caches. In *2017 IEEE International Symposium on High Performance Computer Architecture (HPCA)*, pages 481–492, Feb 2017.
- [3] J. Albericio, A. Delmás, P. Judd, S. Sharify, G. O’Leary, R. Genov, and A. Moshovos. Bit-pragmatic deep neural network computing. In *Proceedings of the 50th Annual IEEE/ACM International Symposium on Microarchitecture*, MICRO-50 '17, pages 382–394, New York, NY, USA, 2017. ACM.
- [4] J. Albericio, P. Judd, T. Hetherington, T. Aamodt, N. E. Jerger, and A. Moshovos. Cnvlutin: Ineffectual-neuron-free deep neural network computing. In *Proceedings of the 43rd International Symposium on Computer Architecture*, ISCA '16, pages 1–13, Piscataway, NJ, USA, 2016. IEEE Press.
- [5] A. Boutros, S. Yazdanshenas, and V. Betz. Embracing diversity: Enhanced dsp blocks for low-precision deep learning on fpgas. In *2018 28th International Conference on Field Programmable Logic and Applications (FPL)*, pages 1–8, Sept 2018.
- [6] S. Cadambi, I. Durdanovic, V. Jakkula, M. Sankaradass, E. Cosatto, S. Chakradhar, and H. P. Graf. A massively parallel fpga-based coprocessor for support vector machines. In *2009 17th IEEE Symposium on Field Programmable Custom Computing Machines*, pages 115–122, April 2009.
- [7] R. Cai, A. Ren, N. Liu, C. Ding, L. Wang, X. Qian, M. Pedram, and Y. Wang. Vibnn: Hardware acceleration of bayesian neural networks. In *Proceedings of the Twenty-Third International Conference on Architectural Support for Programming Languages and Operating Systems*, ASPLOS '18, pages 476–488, New York, NY, USA, 2018. ACM.
- [8] A. M. Caulfield, E. S. Chung, A. Putnam, H. Angepat, J. Fowers, M. Haselman, S. Heil, M. Humphrey, P. Kaur, J. Kim, D. Lo, T. Massengill, K. Ovtcharov, M. Papamichael, L. Woods, S. Lanka, D. Chiou, and D. Burger. A cloud-scale acceleration architecture. In *2016 49th Annual IEEE/ACM International Symposium on Microarchitecture (MICRO)*, pages 1–13, Oct 2016.
- [9] A. M. Caulfield, E. S. Chung, A. Putnam, H. Angepat, J. Fowers, M. Haselman, S. Heil, M. Humphrey, P. Kaur, J. Y. Kim, D. Lo, T. Massengill, K. Ovtcharov, M. Papamichael, L. Woods, S. Lanka, D. Chiou, and D. Burger. A cloud-scale acceleration architecture. In *2016 49th Annual IEEE/ACM International Symposium on Microarchitecture (MICRO)*, pages 1–13, Oct 2016.
- [10] C.-C. Chang and C.-J. Lin. Libsvm: A library for support vector machines. *ACM Trans. Intell. Syst. Technol.*, 2(3):27:1–27:27, May 2011.
- [11] J. W. A. S. R. I. D. S. D. B. R. D. Charles Eckert, Xiaowei Wang. Neural cache: Bit-serial in-cache acceleration of deep neural networks. In *Proceedings of the 44th Annual International Symposium on Computer Architecture*, ISCA '18. ACM, 2018.
- [12] Y. Chen, T. Luo, S. Liu, S. Zhang, L. He, J. Wang, L. Li, T. Chen, Z. Xu, N. Sun, and O. Temam. Dadiannao: A machine-learning supercomputer. In *2014 47th Annual IEEE/ACM International Symposium on Microarchitecture*, pages 609–622, Dec 2014.
- [13] Y. H. Chen, J. Emer, and V. Sze. Eyeriss: A spatial architecture for energy-efficient dataflow for convolutional neural networks. In *2016 ACM/IEEE 43rd Annual International Symposium on Computer Architecture (ISCA)*, pages 367–379, June 2016.
- [14] Y. H. Chen, T. Krishna, J. S. Emer, and V. Sze. Eyeriss: An energy-efficient reconfigurable accelerator for deep convolutional neural networks. *IEEE Journal of Solid-State Circuits*, 52(1):127–138, Jan 2017.
- [15] Z. Chen, J. Gehrke, and F. Korn. Query optimization in compressed database systems. In *Proceedings of the 2001 ACM SIGMOD International Conference on Management of Data*, SIGMOD '01, pages 271–282, New York, NY, USA, 2001. ACM.
- [16] G. R. Chiu, A. C. Ling, D. Capalija, A. Bitar, and M. S. Abdelfattah. Flexibility: Fpgas and cad in deep learning acceleration. In *Proceedings of the 2018 International Symposium on Physical Design*, ISPD '18, pages 34–41, New York, NY, USA, 2018. ACM.
- [17] E. Chung, J. Fowers, K. Ovtcharov, M. Papamichael, A. Caulfield, T. Massengill, M. Liu, D. Lo, S. Alkalay, M. Haselman, M. Abeydeera, L. Adams, H. Angepat, C. Boehn, D. Chiou, O. Firestein, A. Forin, K. S. Gatlin, M. Ghandi, S. Heil, K. Holohan, A. E. Hussein, T. Juhasz, K. Kagi, R. Kovvuri, S. Lanka, F. van Megen, D. Mukhortov, P. Patel, B. Perez, A. Rapsang, S. Reinhardt, B. Rouhani, A. Sapek, R. Seera, S. Shekar, B. Sridharan, G. Weisz, L. Woods, P. Y. Xiao, D. Zhang, R. Zhao, and D. Burger. Serving dnns in real time at datacenter scale with project brainwave. *IEEE Micro*, 38(2):8–20, Mar 2018.
- [18] M. Courbariaux, Y. Bengio, and J. David. Low precision arithmetic for deep learning. *CoRR*, abs/1412.7024, 2014.
- [19] C. De Sa, M. Feldman, C. Ré, and K. Olukotun. Understanding and optimizing asynchronous low-precision stochastic gradient descent. In *Proceedings of the 44th Annual International Symposium on Computer Architecture*, ISCA '17, pages 561–574, New York, NY, USA, 2017. ACM.
- [20] C. De Sa, M. Leszczynski, J. Zhang, A. Marzoev, C. R. Aberger, K. Olukotun, and C. Ré. High-Accuracy Low-Precision Training. *ArXiv e-prints*, Mar. 2018.
- [21] A. Delmas, S. Sharify, P. Judd, and A. Moshovos. Tartan: Accelerating fully-connected and convolutional layers in deep learning networks by exploiting numerical precision variability. *CoRR*, abs/1707.09068, 2017.
- [22] Z. Du, R. Fasthuber, T. Chen, P. Jenne, L. Li, T. Luo, X. Feng, Y. Chen, and O. Temam. Shidiannao: Shifting vision processing closer to the sensor. In *Proceedings of the 42nd Annual International Symposium on Computer Architecture*, ISCA '15, pages 92–104, New York, NY, USA, 2015. ACM.
- [23] A. Elgohary, M. Boehm, P. J. Haas, F. R. Reiss, and



- B. Reinwald. Compressed linear algebra for large-scale machine learning. *Proc. VLDB Endow.*, 9(12):960–971, Aug. 2016.
- [24] R. Espasa, F. Ardanaz, J. Emer, S. Felix, J. Gago, R. Gramunt, I. Hernandez, T. Juan, G. Lowney, M. Mattina, and A. Sez nec. Tarantula: a vector extension to the alpha architecture. In *Proceedings 29th Annual International Symposium on Computer Architecture*, pages 281–292, 2002.
- [25] F. Farber, N. May, W. Lehner, I. Muller, H. Rauhe, J. Dees, and S. Ag. The sap hana database: An architecture overview, 2012.
- [26] Z. Feng, E. Lo, B. Kao, and W. Xu. Byteslice: Pushing the envelop of main memory data processing with a new storage layout. In *Proceedings of the 2015 ACM SIGMOD International Conference on Management of Data*, SIGMOD '15, pages 31–46, New York, NY, USA, 2015. ACM.
- [27] J. Fowers, K. Ovtcharov, M. Papamichael, T. Massengill, M. Liu, D. Lo, S. Alkalay, M. Haselman, L. Adams, M. Ghandi, S. Heil, P. Patel, A. Sapek, G. Weisz, L. Woods, S. Lanka, S. K. Reinhardt, A. M. Caulfield, E. S. Chung, and D. Burger. A configurable cloud-scale dnn processor for real-time ai. In *2018 ACM/IEEE 45th Annual International Symposium on Computer Architecture (ISCA)*, pages 1–14, June 2018.
- [28] M. Grund, J. Krüger, H. Plattner, A. Zeier, P. Cudre-Mauroux, and S. Madden. Hyrise: A main memory hybrid storage engine. *Proc. VLDB Endow.*, 4(2):105–116, Nov. 2010.
- [29] S. Gupta, A. Agrawal, K. Gopalakrishnan, and P. Narayanan. Deep learning with limited numerical precision. In *Proceedings of the 32nd International Conference on International Conference on Machine Learning - Volume 37*, ICML'15, pages 1737–1746. JMLR.org, 2015.
- [30] N. S. L. L. B. C. J. K. V. C. H. E. H. Sharma, J. Park. Bit fusion: Bit-level dynamically composable architecture for accelerating deep neural networks. In *Proceedings of the 44th Annual International Symposium on Computer Architecture*, ISCA '18. ACM, 2018.
- [31] S. Han, X. Liu, H. Mao, J. Pu, A. Pedram, M. A. Horowitz, and W. J. Dally. Eie: Efficient inference engine on compressed deep neural network. In *Proceedings of the 43rd International Symposium on Computer Architecture*, ISCA '16, pages 243–254, Piscataway, NJ, USA, 2016. IEEE Press.
- [32] S. Han, H. Mao, and W. J. Dally. Deep compression: Compressing deep neural network with pruning, trained quantization and huffman coding. *CoRR*, abs/1510.00149, 2015.
- [33] J. M. Hellerstein, C. Ré, F. Schoppmann, D. Z. Wang, E. Fratkin, A. Gorajek, K. S. Ng, C. Welton, X. Feng, K. Li, and A. Kumar. The madlib analytics library: Or mad skills, the sql. *Proc. VLDB Endow.*, 5(12):1700–1711, Aug. 2012.
- [34] A. L. Holloway, V. Raman, G. Swart, and D. J. DeWitt. How to barter bits for chronons: Compression and bandwidth trade offs for database scans. In *Proceedings of the 2007 ACM SIGMOD International Conference on Management of Data*, SIGMOD '07, pages 389–400, New York, NY, USA, 2007. ACM.
- [35] S. Idreos, F. Groffen, N. Nes, S. Manegold, S. Mullender, and M. Kersten. Monetdb: Two decades of research in column-oriented database. 2012.
- [36] Intel. Intel Arria 10 Device Overview. 2018.
- [37] Z. Istvan, D. Sidler, and G. Alonso. Runtime parameterizable regular expression operators for databases. In *2016 IEEE 24th Annual International Symposium on Field-Programmable Custom Computing Machines (FCCM)*, pages 204–211, May 2016.
- [38] Y. Ji, Y. Zhang, W. Chen, and Y. Xie. Bridge the gap between neural networks and neuromorphic hardware with a neural network compiler. In *Proceedings of the Twenty-Third International Conference on Architectural Support for Programming Languages and Operating Systems*, ASPLOS '18, pages 448–460, New York, NY, USA, 2018. ACM.
- [39] R. Johnson and I. Pandis. The bionic dbms is coming, but what will it look like? In *CIDR*, 2013.
- [40] N. P. Jouppi, C. Young, N. Patil, D. Patterson, G. Agrawal, R. Bajwa, S. Bates, S. Bhatia, N. Boden, A. Borchers, R. Boyle, P.-I. Cantin, C. Chao, C. Clark, J. Coriell, M. Daley, M. Dau, J. Dean, B. Gelb, T. V. Ghaemmamghami, R. Gottipati, W. Gulland, R. Hagmann, C. R. Ho, D. Hogberg, J. Hu, R. Hundt, D. Hurt, J. Ibarz, A. Jaffey, A. Jaworski, A. Kaplan, H. Khaitan, D. Killebrew, A. Koch, N. Kumar, S. Lacy, J. Laudon, J. Law, D. Le, C. Leary, Z. Liu, K. Lucke, A. Lundin, G. MacKean, A. Maggiore, M. Mahony, K. Miller, R. Nagarajan, R. Narayanaswami, R. Ni, K. Nix, T. Norrie, M. Omernick, N. Penukonda, A. Phelps, J. Ross, M. Ross, A. Salek, E. Samadiani, C. Severn, G. Sizikov, M. Snellman, J. Souter, D. Steinberg, A. Swing, M. Tan, G. Thorson, B. Tian, H. Toma, E. Tuttle, V. Vasudevan, R. Walter, W. Wang, E. Wilcox, and D. H. Yoon. In-datacenter performance analysis of a tensor processing unit. In *Proceedings of the 44th Annual International Symposium on Computer Architecture*, ISCA '17, pages 1–12, New York, NY, USA, 2017. ACM.
- [41] P. Judd, J. Albericio, T. Hetherington, T. M. Aamodt, N. E. Jerger, and A. Moshovos. Proteus: Exploiting numerical precision variability in deep neural networks. In *Proceedings of the 2016 International Conference on Supercomputing*, ICS '16, pages 23:1–23:12, New York, NY, USA, 2016. ACM.
- [42] P. Judd, J. Albericio, T. Hetherington, T. M. Aamodt, and A. Moshovos. Stripes: Bit-serial deep neural network computing. In *2016 49th Annual IEEE/ACM International Symposium on Microarchitecture (MICRO)*, pages 1–12, Oct 2016.
- [43] T. Kanungo, D. M. Mount, N. S. Netanyahu, C. D. Piatko, R. Silverman, and A. Y. Wu. An efficient k-means clustering algorithm: Analysis and implementation. *IEEE Transactions on Pattern Analysis Machine Intelligence*, 24:881–892, 07 2002.
- [44] K. Kara, D. Alistarh, G. Alonso, O. Mutlu, and C. Zhang. Fpga-accelerated dense linear machine learning: A precision-convergence trade-off. In *2017 IEEE 25th Annual International Symposium on Field-Programmable Custom Computing Machines (FCCM)*, pages 160–167, April 2017.
- [45] K. Kara, K. Eguro, C. Zhang, and G. Alonso. ColumnML: Column-Store Machine Learning with On-the-Fly Data Transformation. *PVLDB*, 12(4):348–361, 2018.
- [46] K. Kara, J. Giceva, and G. Alonso. Fpga-based data partitioning. In *Proceedings of the 2017 ACM International Conference on Management of Data*, pages 433–445. ACM, 2017.
- [47] V. Karakasis, T. Gkountouvas, K. Kourtis, G. Goumas, and N. Koziris. An extended compression format for the optimization of sparse matrix-vector multiplication. *IEEE*

*Transactions on Parallel and Distributed Systems*, 24(10):1930–1940, Oct 2013.

- [48] J. Kim, M. Sullivan, E. Choukse, and M. Erez. Bit-plane compression: Transforming data for better compression in many-core architectures. In *2016 ACM/IEEE 43rd Annual International Symposium on Computer Architecture (ISCA)*, pages 329–340, June 2016.
- [49] U. Köster, T. Webb, X. Wang, M. Nassar, A. K. Bansal, W. Constable, O. Elibol, S. Gray, S. Hall, L. Hornof, A. Khosrowshahi, C. Kloss, R. J. Pai, and N. Rao. Flexpoint: An adaptive numerical format for efficient training of deep neural networks. In I. Guyon, U. V. Luxburg, S. Bengio, H. Wallach, R. Fergus, S. Vishwanathan, and R. Garnett, editors, *Advances in Neural Information Processing Systems 30*, pages 1742–1752. Curran Associates, Inc., 2017.
- [50] C. Kozyrakis and D. Patterson. Vector vs. superscalar and vliw architectures for embedded multimedia benchmarks. In *35th Annual IEEE/ACM International Symposium on Microarchitecture, 2002. (MICRO-35). Proceedings.*, pages 283–293, 2002.
- [51] C. E. Kozyrakis and D. A. Patterson. Scalable, vector processors for embedded systems. *IEEE Micro*, 23(6):36–45, Nov 2003.
- [52] H. Kwon, A. Samajdar, and T. Krishna. Maeri: Enabling flexible dataflow mapping over dnn accelerators via reconfigurable interconnects. In *Proceedings of the Twenty-Third International Conference on Architectural Support for Programming Languages and Operating Systems, ASPLOS '18*, pages 461–475, New York, NY, USA, 2018. ACM.
- [53] L. Lamport. Multiple byte processing with full-word instructions. *Commun. ACM*, 18(8):471–475, Aug. 1975.
- [54] D. D. Lee and H. S. Seung. Algorithms for non-negative matrix factorization. In T. K. Leen, T. G. Dietterich, and V. Tresp, editors, *Advances in Neural Information Processing Systems 13*, pages 556–562. MIT Press, 2001.
- [55] M. Li, T. Zhang, Y. Chen, and A. J. Smola. Efficient mini-batch training for stochastic optimization. In *Proceedings of the 20th ACM SIGKDD International Conference on Knowledge Discovery and Data Mining, KDD '14*, pages 661–670, New York, NY, USA, 2014. ACM.
- [56] S. Li, C. Xu, Q. Zou, J. Zhao, Y. Lu, and Y. Xie. Pinatubo: A processing-in-memory architecture for bulk bitwise operations in emerging non-volatile memories. In *2016 53rd ACM/EDAC/IEEE Design Automation Conference (DAC)*, pages 1–6, June 2016.
- [57] Y. Li and J. M. Patel. Bitweaving: Fast scans for main memory data processing. In *Proceedings of the 2013 ACM SIGMOD International Conference on Management of Data, SIGMOD '13*, pages 289–300, New York, NY, USA, 2013. ACM.
- [58] Y. Li and J. M. Patel. Widetable: An accelerator for analytical data processing. *Proc. VLDB Endow.*, 7(10):907–918, June 2014.
- [59] D. Liu, T. Chen, S. Liu, J. Zhou, S. Zhou, O. Teman, X. Feng, X. Zhou, and Y. Chen. Pudiannao: A polyvalent machine learning accelerator. In *Proceedings of the Twentieth International Conference on Architectural Support for Programming Languages and Operating Systems, ASPLOS '15*, pages 369–381, New York, NY, USA, 2015. ACM.
- [60] Y. Liu, H. Zhang, L. Zeng, W. Wu, and C. Zhang. Mlbench: Benchmarking machine learning services against human experts. *Proc. VLDB Endow.*, 11(10):1220–1232, June 2018.
- [61] D. Mahajan, J. K. Kim, J. Sacks, A. Ardalani, A. Kumar, and H. Esmaeilzadeh. In-rdbms hardware acceleration of advanced analytics. *Proc. VLDB Endow.*, 11(11):1317–1331, July 2018.
- [62] D. Mahajan, J. Park, E. Amaro, H. Sharma, A. Yazdanbakhsh, J. K. Kim, and H. Esmaeilzadeh. Tabla: A unified template-based framework for accelerating statistical machine learning. In *2016 IEEE International Symposium on High Performance Computer Architecture (HPCA)*, pages 14–26, March 2016.
- [63] B. Moons and M. Verhelst. A 0.3 x2013;2.6 tops/w precision-scalable processor for real-time large-scale convnets. In *2016 IEEE Symposium on VLSI Circuits (VLSI-Circuits)*, pages 1–2, June 2016.
- [64] T. Moreau, M. Wyse, J. Nelson, A. Sampson, H. Esmaeilzadeh, L. Ceze, and M. Oskin. Snnap: Approximate computing on programmable socs via neural acceleration. In *2015 IEEE 21st International Symposium on High Performance Computer Architecture (HPCA)*, pages 603–614, Feb 2015.
- [65] P. O’Neil and D. Quass. Improved query performance with variant indexes. In *Proceedings of the 1997 ACM SIGMOD International Conference on Management of Data, SIGMOD '97*, pages 38–49, New York, NY, USA, 1997. ACM.
- [66] M. Owaid, D. Sidler, K. Kara, and G. Alonso. Centaur: A framework for hybrid cpu-fpga databases. In *2017 IEEE 25th Annual International Symposium on Field-Programmable Custom Computing Machines (FCCM)*, pages 211–218, April 2017.
- [67] O. Polychroniou and K. A. Ross. Efficient lightweight compression alongside fast scans. In *Proceedings of the 11th International Workshop on Data Management on New Hardware, DaMoN'15*, pages 9:1–9:6, New York, NY, USA, 2015. ACM.
- [68] V. Raman, G. Swart, L. Qiao, F. Reiss, V. Dialani, D. Kossmann, I. Narang, and R. Sidle. Constant-time query processing. In *Proceedings of the 2008 IEEE 24th International Conference on Data Engineering, ICDE '08*, pages 60–69, Washington, DC, USA, 2008. IEEE Computer Society.
- [69] B. Reagen, P. Whatmough, R. Adolf, S. Rama, H. Lee, S. K. Lee, J. M. Hernández-Lobato, G.-Y. Wei, and D. Brooks. Minerva: Enabling low-power, highly-accurate deep neural network accelerators. In *Proceedings of the 43rd International Symposium on Computer Architecture, ISCA '16*, pages 267–278, Piscataway, NJ, USA, 2016. IEEE Press.
- [70] B. Recht, C. Re, S. Wright, and F. Niu. Hogwild: A lock-free approach to parallelizing stochastic gradient descent. In J. Shawe-Taylor, R. S. Zemel, P. L. Bartlett, F. Pereira, and K. Q. Weinberger, editors, *Advances in Neural Information Processing Systems 24*, pages 693–701. Curran Associates, Inc., 2011.
- [71] D. Rinfret, P. O’Neil, and E. O’Neil. Bit-sliced index arithmetic. In *Proceedings of the 2001 ACM SIGMOD International Conference on Management of Data, SIGMOD '01*, pages 47–57, New York, NY, USA, 2001. ACM.
- [72] R. M. Russell. The cray-1 computer system. *Commun. ACM*, 21(1):63–72, Jan. 1978.
- [73] B. Schlegel, R. Gemulla, and W. Lehner. Fast integer compression using simd instructions. In *Proceedings of the*

- Sixth International Workshop on Data Management on New Hardware*, DaMoN '10, pages 34–40, New York, NY, USA, 2010. ACM.
- [74] V. Seshadri, D. Lee, T. Mullins, H. Hassan, A. Boroumand, J. Kim, M. A. Kozuch, O. Mutlu, P. B. Gibbons, and T. C. Mowry. Ambit: In-memory accelerator for bulk bitwise operations using commodity dram technology. In *Proceedings of the 50th Annual IEEE/ACM International Symposium on Microarchitecture*, MICRO-50 '17, pages 273–287, New York, NY, USA, 2017. ACM.
- [75] H. Sharma, J. Park, D. Mahajan, E. Amaro, J. K. Kim, C. Shao, A. Mishra, and H. Esmaeilzadeh. From high-level deep neural models to fpgas. In *2016 49th Annual IEEE/ACM International Symposium on Microarchitecture (MICRO)*, pages 1–12, Oct 2016.
- [76] D. Sidler, Z. István, M. Owaid, and G. Alonso. Accelerating pattern matching queries in hybrid cpu-fpga architectures. In *Proceedings of the 2017 ACM International Conference on Management of Data*, SIGMOD '17, pages 403–415, New York, NY, USA, 2017. ACM.
- [77] D. Sidler, Z. István, M. Owaid, K. Kara, and G. Alonso. doppiodb: A hardware accelerated database. In *Proceedings of the 2017 ACM International Conference on Management of Data*, pages 1659–1662. ACM, 2017.
- [78] A. Sinha and A. P. Chandrakasan. Energy efficient filtering using adaptive precision and variable voltage. In *Twelfth Annual IEEE International ASIC/SOC Conference (Cat. No. 99TH8454)*, pages 327–331, 1999.
- [79] V. Sze, Y. H. Chen, T. J. Yang, and J. S. Emer. Efficient processing of deep neural networks: A tutorial and survey. *Proceedings of the IEEE*, 105(12):2295–2329, Dec 2017.
- [80] J. Teubner and L. Woods. *Data Processing on FPGAs Synthesis Lectures on Data Management*. Morgan & Claypool, 2013.
- [81] P. F. Thomas Willhalm, Roman Dementiev. Intel Performance Counter Monitor - A better way to measure CPU utilization. Technical report, Intel, 2016.
- [82] Y. Umuroglu, N. J. Fraser, G. Gambardella, M. Blott, P. Leong, M. Jahre, and K. Vissers. Finn: A framework for fast, scalable binarized neural network inference. In *Proceedings of the 2017 ACM/SIGDA International Symposium on Field-Programmable Gate Arrays*, pages 65–74. ACM, 2017.
- [83] Y. Umuroglu, L. Rasnayake, and M. Sjlander. Bismo: A scalable bit-serial matrix multiplication overlay for reconfigurable computing. In *2018 28th International Conference on Field Programmable Logic and Applications (FPL)*, pages 307–3077, Aug 2018.
- [84] K. S. H. E. R. G. V. Akhlaghi, A. Yazdanbakhsh. Snapea: Predictive early activation for reducing computation in deep convolutional neural networks. In *Proceedings of the 44th Annual International Symposium on Computer Architecture*, ISCA '18. ACM, 2018.
- [85] J. Wang and G. Joshi. Adaptive communication strategies to achieve the best error-runtime trade-off in local-update SGD. *CoRR*, abs/1810.08313, 2018.
- [86] Z. Wang, B. He, and W. Zhang. A study of data partitioning on opencl-based fpgas. In *2015 25th International Conference on Field Programmable Logic and Applications (FPL)*, pages 1–8, Sept 2015.
- [87] Z. Wang, J. Paul, H. Y. Cheah, B. He, and W. Zhang. Relational query processing on opencl-based fpgas. In *2016 26th International Conference on Field Programmable Logic and Applications (FPL)*, pages 1–10, Aug 2016.
- [88] Z. Wang, J. Paul, B. He, and W. Zhang. Multikernel data partitioning with channel on opencl-based fpgas. *IEEE Transactions on Very Large Scale Integration (VLSI) Systems*, 25(6):1906–1918, June 2017.
- [89] Z. Wang, K. Zhang, H. Zhou, X. Liu, and B. He. Hebe: An order-oblivious and high-performance execution scheme for conjunctive predicates. In *2018 IEEE 34th International Conference on Data Engineering (ICDE)*, pages 1260–1263, April 2018.
- [90] K. Q. Weinberger, A. Dasgupta, J. Attenberg, J. Langford, and A. J. Smola. Feature hashing for large scale multitask learning. *CoRR*, abs/0902.2206, 2009.
- [91] T. Westmann, D. Kossmann, S. Helmer, and G. Moerkotte. The implementation and performance of compressed databases. *SIGMOD Rec.*, 29(3):55–67, Sept. 2000.
- [92] S. A. White. Applications of distributed arithmetic to digital signal processing: a tutorial review. *IEEE ASSP Magazine*, 6(3):4–19, July 1989.
- [93] T. Xanthopoulos and A. Chandrakasan. A low-power dct core using adaptive bitwidth and arithmetic activity exploiting signal correlations and quantization. In *1999 Symposium on VLSI Circuits. Digest of Papers (IEEE Cat. No. 99CH36326)*, pages 11–12, June 1999.
- [94] J. Yu, A. Lukefahr, D. Palframan, G. Dasika, R. Das, and S. Mahlke. Scalpel: Customizing dnn pruning to the underlying hardware parallelism. In *Proceedings of the 44th Annual International Symposium on Computer Architecture*, ISCA '17, pages 548–560, New York, NY, USA, 2017. ACM.
- [95] C. Zhang and C. Ré. Dimmwithd: A study of main-memory statistical analytics. *Proc. VLDB Endow.*, 7(12):1283–1294, Aug. 2014.
- [96] H. Zhang, J. Li, K. Kara, D. Alistarh, J. Liu, and C. Zhang. ZipML: Training linear models with end-to-end low precision, and a little bit of deep learning. In D. Precup and Y. W. Teh, editors, *Proceedings of the 34th International Conference on Machine Learning*, volume 70 of *Proceedings of Machine Learning Research*, pages 4035–4043, International Convention Centre, Sydney, Australia, 06–11 Aug 2017. PMLR.
- [97] M. Zinkevich, M. Weimer, L. Li, and A. J. Smola. Parallelized stochastic gradient descent. In J. D. Lafferty, C. K. I. Williams, J. Shawe-Taylor, R. S. Zemel, and A. Culotta, editors, *Advances in Neural Information Processing Systems 23*, pages 2595–2603. Curran Associates, Inc., 2010.

## 11. APPENDIX

### 11.1 Cost Model

In this section, we propose a hybrid analytical/empirical cost model to predict the performance of MLWeaving on FPGAs. We predict the throughput  $Th$  to be the minimum value between computing throughput  $Th_{comp}$  and memory throughput  $Th_{mem}$ , as shown in Equation 6.

$$Th = \text{Min}(Th_{comp}, Th_{mem}) \quad (6)$$

#### 11.1.1 Evaluating Computing Throughput

In this subsection, we present an analytical model to evaluate the computing throughput for “chaining” and “no chaining”, under one assumption that the memory subsystem can provide the data as soon as the computing logic requires. The MLWeaving hardware design can consume 512 bits per cycles, so its theoretical computing throughput is  $512 \text{ bits} \times 400 \text{ MHz} = 25.6 \text{ GB/s}$ . However, the practical computing throughput is lower, since MLWeaving has to guarantee the RAW dependency regarding the model. One unavoidable factor is the pipeline latency  $L$ , which is distance between dot product and model updating modules. Its value is  $40 + 2s$  cycles, where  $s$  is the precision level.

“**Chaining**”. We evaluate the computing throughput of “chaining”, as shown in Equation 7.

$$Th_{comp} = \frac{(B/8) \times \lceil M/64 \rceil \times s}{(B/8) \times \lceil M/64 \rceil \times s + L} \times 25.6 \text{ GB/s}, \quad (7)$$

where the right part is the theoretical computing throughput and the left part is the utilization of the computing logic (i.e., dot product module). Since the chaining is enabled, the overhead of model updating can be removed. However, the pipeline latency  $L$  cannot be ignored, especially when  $M$  and  $s$  are small.

“**No chaining**”. Now we evaluate the computing throughput of “no chaining”, as shown in Equation 8.

$$Th_{comp} = \frac{(B/8) \times \lceil M/64 \rceil \times s}{(1 + B/8) \times \lceil M/64 \rceil \times s + L} \times 25.6 \text{ GB/s}, \quad (8)$$

where the overhead of model updating is  $\lceil M/64 \rceil \times s$ . The main difference from “chaining” is that its dot product is idle when the model updating is active.

#### 11.1.2 Evaluating Memory Throughput

MLWeaving accesses the host memory via two PCIe and one QPI links, so the memory throughput is impacted by both memory subsystem and PCIe/QPI links. This makes the explicit prediction (in terms of analytical cost model) of memory throughput extremely difficult, especially under the condition the memory-related IP core on the FPGA side is encrypted. Therefore, we present an empirical cost model to evaluate the memory throughput  $Th_{mem}$ . In order to predict the memory throughput of MLWeaving, we analyze the memory access pattern of MLWeaving and then benchmark the memory throughput. Note, both “chaining” and “no chaining” have the same memory subsystem.

**Memory Access Pattern.** The memory access pattern of MLWeaving is quite fixed. Essentially, for the precision level  $s$ , it sequentially fetch  $s$  cache lines (512 bits) every 32 cache lines, regardless of the number of features. We conclude that its memory bandwidth is quite fixed.

**Benchmarking Memory Throughput.** Based on the memory access pattern, we can benchmark the memory throughput for each precision level  $s$  under our framework Centaur [66]. We can get the empirical memory throughput, as illustrated in Equation 9. We can observe that when  $s$  is small (e.g.,  $< 4$ ), the memory throughput

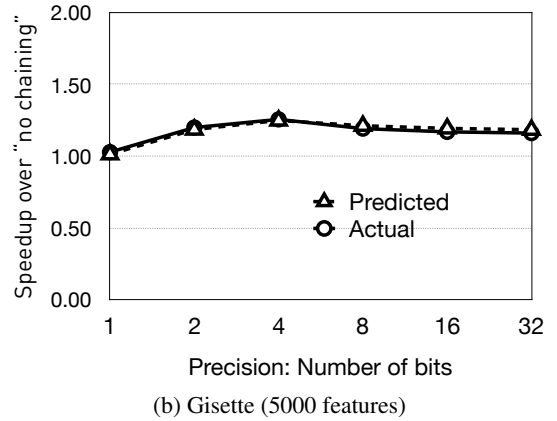
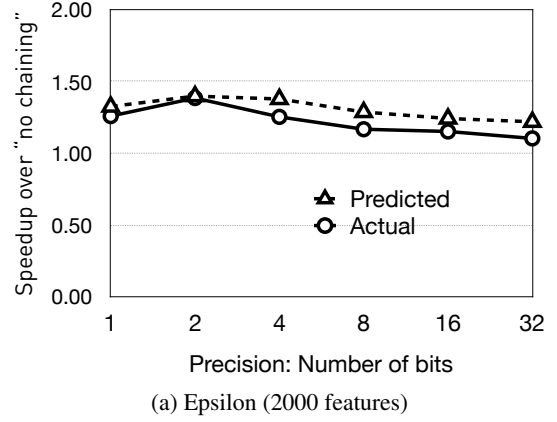


Figure 16: Speedup of “chaining” over “no chaining”.

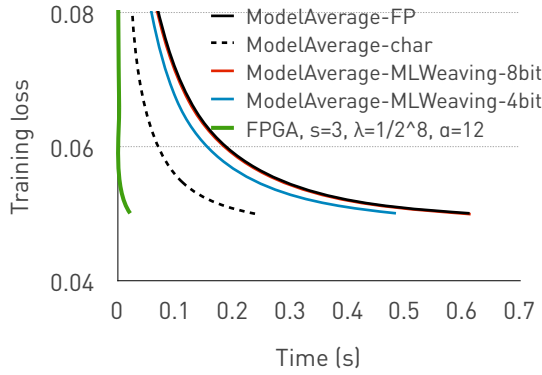
becomes noticeably lower due to its low utilization of row buffer contents. When  $s$  is larger than 4, the throughput of PCIe/QPI links becomes the new bottleneck, so the achievable throughput stays the same.

$$Th_{mem} = \begin{cases} 10.2 \text{ GB/s} & s = 1 \\ 13.3 \text{ GB/s} & s = 2 \\ 13.8 \text{ GB/s} & s = 3 \\ 14.8 \text{ GB/s} & s \geq 4 \end{cases} \quad (9)$$

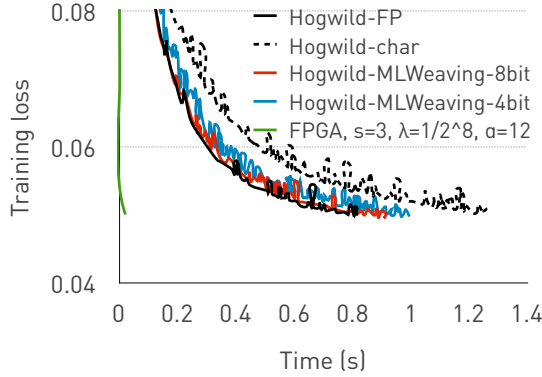
#### 11.1.3 Predicting MLWeaving Performance via Cost Model

In this subsection, we leverage our cost model to predict the speedup of chaining over no chaining to demonstrate the effect of chaining. Actually, the intuition behind this speedup is not straightforward. In order to understand this speedup, we leverage our cost model to predict the throughput of chaining and no chaining individually. Then, we can calculate the speedup to be the throughput ( $Th$ ) of chaining divided by the throughput ( $Th$ ) of no chaining with different number of features ( $M$ ) and different precision level ( $s$ ), and then we can get the different peak speed up for different dataset, as shown in Figure 16. “Actual” indicates the real speedup number from our experiment, while “predicted” indicates the number from our cost model. We make two observations.

First, our cost model can roughly predict the speedup for different precision. Second, our cost model can predict the peak speedup for different number of features ( $M$ ) and different precision level ( $s$ ). In particular, the peak speedup is for  $s=4$  for Epsilon (2K features), while the peak is at  $s=2$  for Gisette (5k features). We con-



(a) ModelAverage,  $\lambda = 1/2^8$ ,  $\beta = 0.98$



(b) Hogwild,  $\lambda = 1/2^{11}$ ,  $\alpha = 12$

Figure 17: MLWeaving on CPU with the dataset of Epsilon.

clude that our cost model can guide us to find the peak speedup with different precision level and different number of features.

## 11.2 MLWeaving on Modern CPUs

We examine the performance of MLWeaving on CPUs. Since modern CPU does not yet have any custom instructions to efficiently consume the bit stream from MLWeaving layout, we have to employ normal instructions to retrieve the data for further computing. For instance, the 8-bit element contains bits from eight different memory locations, indicating quite significant lookup overhead. We make our best effort that our implementation is able to retrieve 32 elements (i.e., 32-way parallelism) in a single AVX2 instruction. Figure 17 illustrates the performance of MLWeaving on CPUs. We can make three observations.

First, MLWeaving can be faster than the floating-point implementation under ModelAverage, when the precision level is less than 8 bits, as shown in Figure 17a. It means that MLWeaving can also bring reasonable benefit on CPUs. Second, MLWeaving makes low-precision implementation slower under ModelAverage. In particular, “ModelAverage-MLWeaving-8-bit” is much slower than “ModelAverage-char”, even though both have the same precision of 8 bits. It means that the lookup overhead from MLWeaving cannot be fully amortized when deploying on CPUs. Third, the low-precision implementation makes HogWild slower, as HogWild is always bounded by cache coherence overhead. It means that low-precision implementation, which can generate more shared model updating operations in a fixed period, incurs more pressure to cache coherence module inside a CPU.

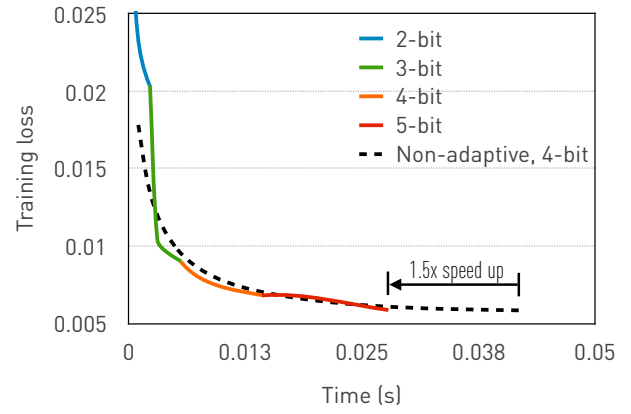


Figure 18: Impact of flexible precision schedule.

## 11.3 Flexible Precision Schedule

Figure 18 shows the per-epoch tuning process for Giset dataset. The x-axis is the elapsed time and the y-axis is the training loss. The baseline here is the 4-bit precision, denoted by “Non-adaptive, 4-bit”, which can converge to the same training loss as full precision does. The proposed adaptive approach increases the level of precision during the training. In particular, it starts with 2-bit precision (denoted by “2-bit”) for the first four epochs, followed by four epochs for 3-bit precision (denoted by “3-bit”). Then, 4-bit is used for the next eight epochs. Finally, ten epochs are employed under 5-bit precision to reach the target loss. We can draw two observations.

First, the proposed flexible precision schedule can reach the same training loss, while achieving 1.5X performance improvement over the baseline (“Non-adaptive, 4-bit”), even though the schedule is preliminary, indicating a great potential of per-epoch precision schedule. Second, each precision level transition (e.g., 2-bit to 3-bit) brings a significant reduction in loss, coinciding with our theory that tuning the precision level higher (e.g., 2-bit to 3-bit) at runtime can converge to the same loss as a fixed 3-bit precision for all the epochs.

## 11.4 Convergence Analysis

We add the experiment result for the remaining three datasets, as shown in Figure 19.



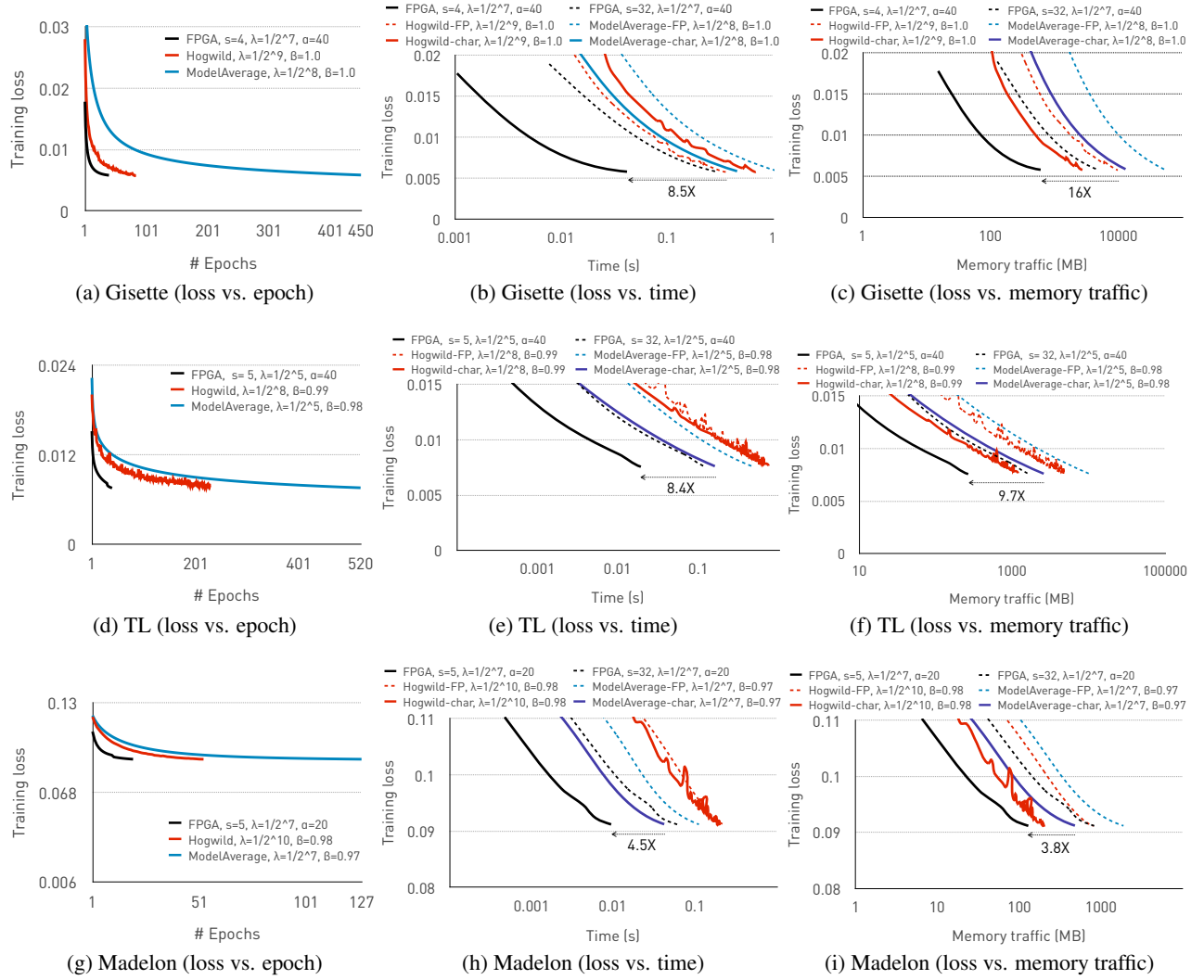


Figure 19: Convergence comparison: loss vs. epoch/time/memory traffic. The batch size is 8. Speedup indicates MLWeaving vs. fastest 14-core AVX2-enhanced low-precision CPU approach, in terms of time and memory traffic.